Refining the signature of thallium isotopes in low oxygen marine environments

Sean M. Newby [a,c,*], Siqi Li [b,c], Silke Severmann [d], James McManus [e], Florian Scholz [f], Jeremy D. Owens [c]

[a] Department of Earth and Planetary Sciences, University of Hong Kong, Hong Kong, China
[b] Department of Earth and Planetary Sciences, University of California Riverside, Riverside, CA 92521, USA
[c] Earth, Ocean, and Atmospheric Science Department, National High Magnetic Field Laboratory, Florida State University, Tallahassee, FL 32304, USA
[d] Department of Marine and Coastal Sciences, School of Environmental and Biological Sciences, Rutgers University, New Brunswick, NJ 08901, USA
[e] Bigelow Laboratory for Ocean Sciences, East Boothbay, Maine 04544, USA
[f] Institute for Geology, Center for Earth System Research and Sustainability, Universität Hamburg 20146 Hamburg, Germany

ARTICLE INFO

ABSTRACT

Thallium (Tl) isotopic values (ε^{205}Tl) appear to track changes in marine manganese oxide deposition, with these isotope signatures having been utilized as a proxy for rapid oceanic seafloor (de-)oxygenation events. With a residence time longer than ocean mixing time and the ability to track the deposition of manganese oxides, ε^{205}Tl may effectively record the earliest global transitions in the extent of ocean oxygenation. However, some uncertainty remains for the minor Tl sinks in degree of fractionation from seawater values, if any, with the limited data currently available suggesting at least a 6 epsilon unit range in fractionation from seawater values in low oxygen environments. This study provides Tl data for sediment cores from a range of low-oxygen marine environments. With these data, we identify potential processes that impact the range of Tl isotope variations within the sediments, which are not all due to local Mn oxide cycling. Previous work indicates that euxinic (anoxic and sulfidic water column) conditions and early diagenetic pyrite formed under consistently anoxic sediments record seawater values with no (or not measurable) fractionation during absorption to pyrite. Our new data provide downcore confirmation. Meanwhile, only limited data from 'suboxic' environments (those with low oxygen but likely not permanently anoxic conditions) has been analyzed. Thus, isotopic data for suboxic systems is needed to refine the current mass balance. Several sites off the California, Mexico, and Peru coasts with a range of redox states from oxic to perennially anoxic were selected to allow for a comparison across a range of open ocean bottom water conditions. The locations with oxic sediments tend to document more positive values compared to seawater, as expected due to local manganese oxide incorporation. Sediments from more 'suboxic' (manganous to ferruginous) sites tend to have invariable downcore geochemical signatures that are between marine inputs (−2) and modern seawater (−6) values, indicating a mixing of ε^{205}Tl signatures from different authigenic phases; however, these are not primarily due to the incorporation of Mn oxides as the concentrations are low and uncorrelated. The anoxic sites record Tl isotope compositions near seawater values, confirming that early diagenetically formed pyrite (and precursor minerals) record seawater ε^{205}Tl signatures under permanent anoxia. Importantly, these permanently anoxic localities have minor Mn contents, which suggest no local Mn oxide Tl isotope signatures. Therefore, unlike the anoxic sediments, the 'suboxic' sediments have a Tl isotope value that is slightly offset from seawater without significant Mn oxide deposition, thus suggesting there could be a fractionation for this process. Our observations provide improved constraints on the Tl isotope system, especially on a poorly constrained aspect of the mass balance, which will be important for deep-time applications.

* Corresponding author at: Department of Earth and Planetary Sciences, University of Hong Kong, Hong Kong, China.
  E-mail address: snewby@hku.hk (S.M. Newby).

1. Introduction

Throughout Earth's history, changes in the molecular oxygen content of the atmosphere and oceans have been a major control on biotic development (Berner, 2001; Lyons et al., 2014). There is evidence that substantial (de-)oxygenation is an important contributing factor to prominent biological diversification intervals as well as many of the largest extinction events of the Phanerozoic (Poulton and Canfield, 2005; Canfield et al., 2007; Hardisty et al., 2014; Lyons et al., 2014; Bond and Grasby, 2017; Them et al., 2018; Bowman et al., 2019; Ostrander et al., 2019; Fan et al., 2020; Li et al., 2021; Newby et al., 2021; Kozik et al., 2022, 2023). However, there is no direct means to measure oxygen content in the geologic past, requiring geochemical and paleontological proxies to interpret changes in marine oxygen over ancient time intervals (Froelich et al., 1979; Owens, 2019).

One of the most notable elements affected by changes in the redox state of the ocean is manganese (Mn), primarily in the form of Mn oxides such as birnessite (Rue et al., 1994). Manganese oxides are some of the earliest major minerals to start forming during oxygenation of the water column and some of the first to remineralize from the seafloor under low oxygen conditions, both because of Mn's high reduction potential during the transformation from Mn(IV) to Mn(II) that can be mediated or accelerated by microbial activity (Froelich et al., 1979; Algeo and Maynard, 2004; Tribovillard et al., 2006; Lu et al., 2010; Hansel, 2017; Owens, 2019; Liu et al., 2020). Due to this close relationship with seawater dissolved oxygen content, Mn is an important element that can track changes in oceanic redox conditions. However, this element has a short residence time (~60 years) in the modern ocean (Tribovillard et al., 2006), primarily due to its rapid utilization in an oxic water column to form Mn oxides (Algeo and Maynard, 2004), and it has only one stable, geologically long-lived isotope, making it difficult to track global chemical changes across geologic timescales.

Many redox-sensitive elements (e.g., vanadium, nickel, zinc, molybdenum, thallium, and uranium) are adsorbed onto or structurally incorporated into Mn oxides (Algeo and Maynard, 2004; Tribovillard et al., 2006). Additionally, these elements have long residence times and multiple isotopes that can fractionate during the adsorption/incorporation processes (Algeo and Maynard, 2004; Tribovillard et al., 2006; Kendall et al., 2017; Nielsen et al., 2017; Owens, 2019; Wu et al., 2019; Lau et al., 2019; Nielsen, 2021). Therefore, the isotope systems associated with these elements are potential tools for constraining global changes in redox conditions (Kendall et al., 2017; Lau et al., 2019; Nielsen, 2021). Thallium (Tl) isotopes have a large fractionation associated with Mn oxides, specifically birnessite; thus, understanding the redox state of the sediments and the associated Tl isotope signature is important to build confidence in the proxy. The Tl isotope (ε^{205}Tl) signature of sediments has been used as a relatively novel paleoredox proxy that has been developed over the last couple of decades (Rehkämper et al., 2002; Rehkämper and Nielsen, 2004; Nielsen et al., 2004, 2005, 2006c, b, 2007, 2013; Baker et al., 2009; Prytulak et al., 2013; Owens et al., 2017; Chen et al., 2021; Wang et al., 2022; Ostrander et al., 2023, 2024) and has been utilized for several intervals throughout Earth's history (Ostrander et al., 2017, 2019, 2023; Them et al., 2018; Bowman et al., 2019; Newby et al., 2021; Li et al., 2021; Kozik et al., 2022, 2023; Heard et al., 2023). There are multiple reviews of the low temperature Tl isotope system (Nielsen et al., 2017; Owens, 2019), so only the most germane points will be covered here.

Thallium has two stable isotopes, the lighter ^{203}Tl and heavier ^{205}Tl. The Tl isotopic composition is reported as:

$$\varepsilon^{205}\text{Tl} = \left(^{205}\text{Tl}/^{203}\text{Tl}_{\text{sample}} - {}^{205}\text{Tl}/^{203}\text{Tl}_{\text{NIST-SRM-997}}\right) \Big/ \left(^{205}\text{Tl}/^{203}\text{Tl}_{\text{NIST-SRM-997}}\right) \times 10,000,$$

which utilizes the NIST-SRM-997 Tl metal standard and is reported in dimensionless epsilon (ε) units. With an estimated residence time of 18.5 kyr, Tl is well-mixed in the modern ocean (oceanic mixing time is

~1–2 kyr), making open ocean ε^{205}Tl values homogenous at ~−6.0 (Rehkämper et al., 2002; Nielsen et al., 2006c; Owens et al., 2017).

The various sources of Tl to the marine reservoir have similar isotopic compositions of ~−2.0, and as a result changes in the relative supply of these sources have a minor impact on changing the seawater composition (Rehkämper et al., 2002; Rehkämper and Nielsen, 2004; Nielsen et al., 2005, 2006c, 2007, 2011, 2016; Baker et al., 2009; Prytulak et al., 2013). The result of having this consistent Tl source composition is that the marine ε^{205}Tl value is likely controlled by the fractionating sinks (Rehkämper et al., 2002; Nielsen et al., 2004, 2006b, 2017; Rehkämper and Nielsen, 2004; Prytulak et al., 2013; Owens, 2019). The Mn oxide sink in particular is notable due to its large positive isotopic value (~+10.0) and the potential to be included in various marine sediments such as the ones in this study (Rehkämper et al., 2002; Rehkämper and Nielsen, 2004; Nielsen et al., 2006b). Alteration of oceanic crust is the other major sink with a larger flux but relatively smaller negative fractionation from seawater (~−1.2), which limits its isotopic effect on oceanic composition.

Though much smaller, the two reducing sinks, those depositing Tl under suboxic conditions and under anoxic-euxinic conditions, are the focus of this study due to their relevance as sedimentary archives of ancient seawater isotopic compositions. The most faithful records of seawater ε^{205}Tl are found under euxinic conditions, where Tl quantitatively adsorbs onto precipitating pyrite and records seawater values (Owens et al., 2017). Further research has shown that an anoxic water column, where pyrite formation occurs to a lesser extent within the sediments than under euxinic conditions, can also accurately record the overlying seawater Tl isotopic values if the pore waters remain sufficiently sulfide-rich (Fan et al., 2020), and other research indicates quantitative removal is not necessary for sulfides to record seawater isotopic composition (Ostrander et al., 2023). Wang et al. (2022) has also shown that there are a variety of reducing conditions that can record seawater values without necessitating measurement of sulfides, unlike most previous studies (Nielsen et al., 2011; Owens et al., 2017), as long as certain other redox conditions are met, including enrichments of notable productivity- and redox-sensitive trace elements (barium and uranium) and lack of manganese oxide formation. However, the least well-constrained sink of Tl remains burial under suboxic conditions, with little data from these types of environments (Rehkämper and Nielsen, 2004; Nielsen et al., 2011; Owens et al., 2017) and these environments containing a potentially large range of values (Owens, 2019; Wang et al., 2022). This study aims to better constrain how specific redox conditions, especially the generalized zones of suboxic and anoxic depositional conditions, can affect the recorded Tl isotope signature and how this record may affect future use of this proxy.

To further explore the broad term of 'suboxia', a range of definitions can be considered. For our purposes, suboxic sedimentary conditions are those where the processes of denitrification, Mn and iron (Fe) reduction, and sulfate reduction, occur in within the near surface sediment package despite bottom waters that have a low (0.2–2.0 mL/L, ~6–60 μM) or zero O_2 content (Tyson and Pearson, 1991; Algeo and Maynard, 2004). These environments are often enriched in many trace metal concentrations with a decrease in sedimentary Mn and Fe concentrations (Algeo and Maynard, 2004; Tribovillard et al., 2006). This categorization covers various geochemical redox states and can be applied to both water column and porewater conditions, and we apply this terminology here to remain consistent with previous Tl isotope work employing this terminology (Nielsen et al., 2011, 2013, 2017; Owens et al., 2017; Owens, 2019) In addition, redox-uncertainty for deep-time sedimentary records has also resulted in potential need for classification as suboxic as there is limited proxy specificity due to early diagenesis compared to modern research. However, to further geochemically define our modern sediments, additional classifications based on porewater and sediment compositions are necessary, including in order of decreasing redox potential: dissolved Mn-rich manganous conditions, dissolved Fe-rich ferruginous conditions, and hydrogen sulfide-rich sulfidic conditions
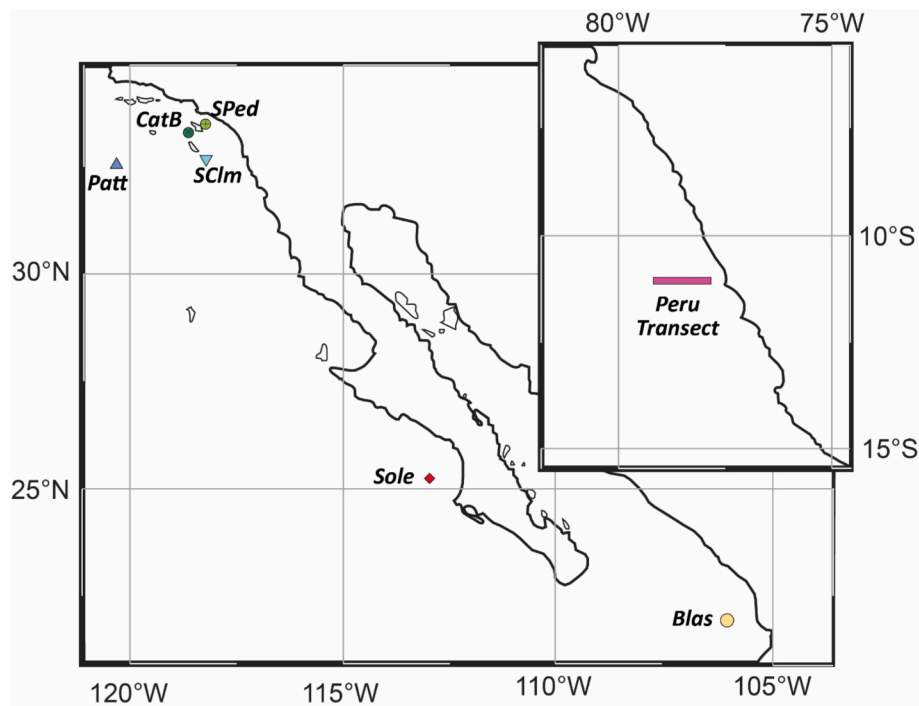
ARTICLE IN PRESS

S.M. Newby et al.   Geochimica et Cosmochimica Acta xxx (xxxx) xxx

Fig. 1. Locality map of stations utilized for the study. Main map is of the California and Mexico Margin with six sites utilized. Inset is of the Peru Margin using a transect of material that includes various sites too close to differentiate. See Table 1 for precise coordinates of all sites. Colors and shapes are intended to match Figs. 2–7. Note that oxic sites are blue triangles, 'suboxic' are yellow to green circles, and anoxic are red to purple squares and diamonds. Blas=San Blas Basin, CatB=Catalina Basin, Patt=Patton Escarpment, SClm=San Clemente Basin, Sole=Soledad Basin, SPed=San Pedro Basin.

Table 1
Descriptions of sites.

Site Location	Longitude	Latitude	Depth	Bottom water O_2	Carbon Burial
	N	W	(m)	(μM)	(mmol/ m²/day)
Patton Escarpment, CA	32.40° N	120.60° W	3707	130	0.08
San Clemente Basin, CA	32.60° N	118.10° W	2053	50	0.9
Catalina Basin, CA	33.30° N	118.60° W	1300	20	1.2 ± 0.3
San Pedro Basin, CA	33.50° N	118.40° W	896	3–8	2.6 ± 0.6
San Blas Basin, Mexico	21.30° N	106.00° W	430	<0.1	8.4 ± 0.3
Soledad Basin, Mexico	25.20° S	112.70° W	542	<0.1	3.2 ± 0.2
BIGO-05, Peru	11.00° S	077.80° W	85	<1.5	
MUC29, Peru	11.00° S	077.94° W	145	<1.5	
MUC33, Peru	11.00° S	078.24° W	376	<1.5	
MUC21, Peru	11.00° S	078.32° W	466	<1.5	
MUC25, Peru	11.00° S	078.43° W	697	12	
MUC15, Peru	11.00° S	078.50° W	928	39	
MUC27, Peru	11.00° S	078.75° W	2025	93.4	

Data from McManus et al. (1997, 1998, 2012), Berelson et al. (2005), Poulson et al. (2006), Scholz et al. (2011, 2014a, 2014b), Chong et al. (2012), Noffke et al. (2012), and Bruggmann et al. (2023).

(Froelich et al., 1979; Owens, 2019). These terms are only applied to porewater samples as the sedimentary samples in this study are focused on the preservation of Tl signatures in sediments; generally, references to the water column will be relegated to the bottom water oxygen content. With these distinctions, references to suboxic conditions will primarily refer to this low oxygen state within the Tl mass balance, while more specific classifications are incorporated into discussion of the studied materials.

2. Samples and Methods

2.1. Sample Collection and Description

In this study, sediments from several marine localities off the coast of California, Mexico, and Peru (Fig. 1) were analyzed for solid phase and porewater Fe and Mn concentrations, to confirm local sedimentary redox conditions, and authigenic Tl isotopes ($\varepsilon^{205}Tl_{auth}$). California-Mexico Margin samples were collected as part of the 1805c cruise (R/V *Oceanus*) in 2018, while the Peru Margin samples were collected as part of the M77-1 and M77-2 cruises (R/V *Meteor*) in 2008. Samples were collected using a multicore device (Barnett et al., 1984). Two cores for every site from six sites in the California-Mexico Margin were collected for sedimentary and porewater analysis of Tl relevant to this study, respectively. Only one sample from Patton Escarpment was collected for just sedimentary analysis due to limitations of time and materials during collection, thereby lacking porewater data. Direct measurements were done at the at the National High Magnetic Field Laboratory (NHMFL) and Florida State University (FSU) facilities. Multiple separate cores per site were processed on-board and analyzed at Rutgers University for bulk porewater collection. A small set of sedimentary sample material from six cores collected during the Peruvian cruise were also utilized, as well as data previously published on these samples (Scholz et al., 2011, 2014a, b). Details of the location, water column depth, and bottom water conditions for all sites can be found in Table 1, but these sites generally cover a range of depths,

bottom water oxygen content, sedimentation rates, and organic carbon burial rates (McManus et al., 1997, 1998, 2012; Berelson et al., 2005; Poulson et al., 2006; Scholz et al., 2014b, 2011, 2014a; Chong et al., 2012; Noffke et al., 2012; Bruggmann et al., 2023).

For each core from the California-Mexico Margin in which sediments were procured, on average, 1 cm slices were taken from the top 10–12 cm of the core, and frozen for later use under laboratory conditions. These samples were all processed at the NHMFL and FSU facilities. Frozen samples were dried in a low-temperature oven (~80 °C) for ~ 12 h and disaggregated using a mortar and pestle to ensure uniform fine-grained material. Portions of each powdered sample were used for bulk sediment trace metal concentrations and Tl isotopic analysis. Descriptions for sediment processing for the Peru Margin can be found in Scholz et al. (2011, 2014a, 2014b).

One core from each site from the California-Mexico Margin except for Patton Escarpment was used to collect a small aliquot of porewater for Tl concentration measurements. After removing the overlying bottom waters from the core, these porewater samples were collected using rhizons inserted into the core approximately every 1 cm through the top 10–12 cm and siphoned out through negative pressure with syringes (Seeberg-Elverfeldt et al., 2005; Chong et al., 2012; Bruggmann et al., 2023). Each sample contained 20 mL of solution with about 80 μL of 12 M HCl added and was kept in sealed conditions until analysis (see Supplemental Discussion). As Tl has such small concentrations in seawater, additional steps were needed to separate out the solutions while also requiring larger quantities of porewater than typically extracted (Section 2.4), which is why this collection was done. For the remaining porewater concentrations, multiple cores were sliced at 1 cm intervals, centrifuged, and the supernatants of the same depth slices for the same site were combined to get sufficient porewater for precise concentration analyses across a larger array of trace metals without needing additional steps. Sample splits were completed aboard R/V Oceanus. These bulk porewater concentrations were then acidified using 12 M HCl and utilized for porewater trace metal concentrations at Rutgers University.

2.2. Bulk Sediment Concentrations

A total digestion procedure similar to other trace metal concentration procedures (Algeo and Maynard, 2004; Tribovillard et al., 2006) was utilized to determine several ancillary elemental concentrations, including aluminum (Al), Mn, Fe, and uranium (U). An aliquot of ~100 mg of powdered sediment was ashed in crucibles in a high temperature oven (~600 °C) for ~12 h. After transferring ashed material into Teflon beakers, a multi-acid procedure incorporating various concentrations and volumes of hydrofluoric acid [HF], nitric acid [HNO$_3$], and hydrochloric acid [HCl] over several days, using hotplates set to 80–160 °C, was utilized until complete dissolution of the sample was accomplished.

Total digestions were analyzed on an Agilent 7500cs quadrupole inductively coupled plasma mass spectrometer (ICP-MS) located at NHMFL's Geochemistry Group to obtain concentration measurements. These were compared to the USGS SDO-1 and SGR-1 standards (Supplemental Table 1) for accuracy of chemical processing methods and analytical accuracy (<5 % error from known concentrations). The total digestion metal concentrations were compared to upper continental crust (UCC) concentrations as a baseline (Mclennan, 2001), including Al (UCC = 8.04 wt%), Mn (UCC = 600 ppm), and Fe (UCC = 3.5 wt%).

2.3. Thallium Column Chemistry

To extract the sedimentary authigenic Tl from pyrite and other reactive mineral phases without the silicate fraction, a standard hot leach was used (Nielsen et al., 2011; Ostrander et al., 2017; Owens et al., 2017). For this procedure, ~100 mg of powdered sediment was weighed out into Teflon beakers and dissolved in 2 M HNO$_3$ at 130 °C for 12 h to

separate the leachable material, herein labeled the authigenic component. The USGS shale reference material SCo-1 was also included in every set of samples to provide analytical and procedural reproducibility. Samples were transferred to centrifuge tubes, centrifuged, and the supernatant was returned to clean Teflon beakers, with the residue saved for lithogenic analysis (see Supplemental Methods). This step was followed by adding a 50:50 mixture of concentrated HNO$_3$–HCl solution to dissolve organic compounds, then transferred to 1 mL 1 M HCl with 100 μL brominated water (Br$_2$-H$_2$O, created from water saturated in bromine) the night prior to column chemistry preparation.

Previously established column chemistry methods using microcolumns filled with Bio-Rad AG1-X8 anion exchange resin to remove Pb from samples were utilized (Nielsen et al., 2004, 2005; Baker et al., 2010b; Ostrander et al., 2017). Column chemistry involved cleaning of resin through progressive steps of 0.1 M HCl–5 % sulfur dioxide [SO$_2$] solution (created by bubbling SO$_2$ through 0.1 M HCl), 0.1 M HCl, and 0.1 M HCl–1 % Br$_2$-H$_2$O. Samples were loaded onto columns and rinsed with 0.5 M HNO$_3$ – 3 % Br$_2$-H$_2$O, 2.0 M HNO$_3$–3 % Br$_2$-H$_2$O, and 0.1 M HCl–1 % Br$_2$-H$_2$O. Solutions were then eluted using 0.1 M HCl–5 % SO$_2$. The eluted material was dried at high temperatures (180–210 °C) to remove SO$_2$, reacted with a 50:50 mixture of concentrated HNO$_3$–HCl solution to dissolve any eluted resin, and reconstituted in 0.1 M HNO$_3$ with 0.1 % sulfuric acid [H$_2$SO$_4$] for analysis.

All samples were analyzed on the NHMFL's Agilent ICP-MS to determine concentrations of Tl and Pb. Samples were then spiked with NIST-SRM-981 Pb solution to track mass-bias during isotope spectrometry analysis (Nielsen et al., 2005). All samples were analyzed on a Neptune multi-collector ICP-MS using an Aridus II autosampler located at the NHMFL to obtain Tl isotopic composition. A standard-sample bracketing analysis was used with NIST-SRM-997 Tl standard being employed for bracketing. Long-term precision of this method is estimated based on the 2SD uncertainty of the SCo-1 reference material, with a known ε^{205}Tl$_{auth}$ of -3.0 ± 0.3 (Ostrander et al., 2017; Owens et al., 2017; Owens, 2019), and our SCo-1 geostandards having ε^{205}Tl$_{auth} = -3.0 \pm 0.4$ (n = 6). All samples were measured at a minimum of two separate analyses to confine uncertainty (two standard deviations, 2SD) to less than 0.5 ε units. All samples with a 2SD error less than 0.3 ε units were rounded up to 0.3 to match the minimum analytical error possible from the long-term geostandard (Owens, 2019).

2.4. Porewater Concentrations

For most Mn and Fe porewater concentrations, aliquots from the collected bulk porewaters were measured using an Agilent ICP-MS at Rutgers University, diluted 20-fold with 2 % HNO$_3$. These samples utilized the bulk collection of porewaters collected from centrifuged slices of sediment under anaerobic conditions. To measure the much lower Tl porewater concentrations without interference from salts in the porewater, greater quantities specifically aliquoted for this analysis were directly obtained with rhizons and additional steps were required to separate out Tl from excess dissolved salts. A similar procedure as Tl column chemistry was utilized on the porewaters due to the method's near complete (>95 %) Tl yield (Ostrander et al., 2017; Owens et al., 2017) to accurately obtain Tl porewater concentrations while removing other dissolved substrates. An aliquot of porewaters from every sample (5 mL) with an additional 0.5 mL of 1 M HCl added was brominated with 250 μL brominated water. Initial Tl column chemistry steps through sample loading were followed. At this point, a rinse with only 0.5 M HNO$_3$–3 % Br$_2$-H$_2$O was done before elution of the sample with 0.1 M HCl–5 % SO$_2$, with other steps unnecessary for just Tl concentration analysis. Procedures following column chemistry were followed and samples were analyzed on the NHMFL Agilent ICP-MS to determine concentrations of Tl in the porewaters. Errors were calculated based on the combined effect of analytical uncertainty and variability within the standard calibration curve associated with the measurement, adding these two uncertainties together to get the potential error of the analysis.

Table 2
Trace metal concentrations and authigenic Tl of samples.

Station	Sample Name	Sediment Depth (cm)	Average Sediment Depth (cm)	Sediment Trace Metal Concentrations			Porewater Trace Metal Concentrations				Authigenic Thallium		
				[Al] bulk (wt%)	[Mn] bulk (ppm)	[Fe] bulk (wt%)	[Mn] pore (µM)	[Fe] pore (µM)	[Tl] pore (pM)	[Tl] error (pM)	[Tl] (ppb)	ε^{205}Tl	error (2SD)
California-Mexico Margin													
Patt*	1805c Patt B3 0–1.2	0–1.2	0.6	6.40	11032.64	4.96	0.01	0.01			793.82	0.66	0.42
	1805c Patt B3 1.2–2.4	1.2–2.4	1.8	6.10	9309.32	4.13	0.02	0.03			808.28	0.82	0.30
	1805c Patt B3 2.4–3.6	2.4–3.6	3.0	6.99	12303.25	5.17	0.02	0.03			805.87	1.56	0.30
	1805c Patt B3 3.6–4.8	3.6–4.8	4.2	11.14	18049.36	8.11	0.23	0.04			465.79	−1.65	0.36
	1805c Patt B3 4.8–6.0	4.8–6.0	5.4	7.33	11147.05	5.00	1.40	0.05			315.11	−2.41	0.30
	1805c Patt B3 6.0–7.2	6.0–7.2	6.6	7.24	7552.85	4.67	5.46	0.04			381.44	−1.99	0.30
	1805c Patt B3 7.2–8.4	7.2–8.4	7.8	6.57	2435.12	4.24	7.22	0.04			335.81	−3.43	0.38
	1805c Patt B3 8.4–9.6	8.4–9.6	9.0	7.21	1951.21	4.39	10.76	0.06			339.58	−3.82	0.36
	1805c Patt B3 9.6–10.8	9.6–10.8	10.2	6.71	1136.15	4.10	8.01	0.06			329.76	−3.69	0.42
	1805c Patt B3 10.8–12.0	10.8–12.0	11.4	7.37	1351.63	4.42	15.35	0.04			692.10	−3.87	0.30
SClm*	1805c SClm C5 0	0	0.0						69.69	4.33			
.	1805c SClm C5 0–2	0–2	1.0	6.77	51153.92	4.16	0.24	0.00	242.64	8.05	584.96	0.85	0.30
	1805c SClm C5 2	2	2.0				12.10	0.09	341.72	14.57			
	1805c SClm C5 2–4	2–4	3.0	7.04	19912.40	4.38	52.51	0.21	437.71	27.74	669.88	−1.83	0.44
	1805c SClm C5 4	4	4.0				92.49	0.32	292.87	13.08			
	1805c SClm C5 4–6	4–6	5.0	7.02	5480.16	4.50	148.77	0.41	172.94	29.54	435.81	−2.87	0.49
	1805c SClm C5 6–8	6–8	7.0	6.98	2471.87	4.46	133.44	5.42	134.02	7.61	397.17	−2.82	0.30
	1805c SClm C5 8–10	8–10	9.0	7.09	2409.32	4.43	156.88	8.50			485.89	−1.57	0.30
	1805c SClm C5 11	11	11.0				146.51		101.66	6.83			
CatB*	1805c CatB A1 0	0	0.0						134.60	6.57			
	1805c CatB A1 0–1	0–1	0.5	5.18	474.95		6.60	0.20	63.26	3.19			
	1805c CatB A1 1–2	1–2	1.5	5.71	1223.95	4.00	14.69	3.50	60.97	2.93	204.45	−4.18	0.43
	1805c CatB A1 2–3	2–3	2.5	5.92	216.13		2.72	10.58	71.19	4.21	239.77	−4.25	0.30
	1805c CatB A1 3–4	3–4	3.5	6.70	761.77	3.91	6.81	11.22	36.64	2.64	290.45	−3.74	0.47
	1805c CatB A1 4–5	4–5	4.5	5.21	160.65		3.40	16.81	19.45	1.95	377.70	−3.98	0.48
	1805c CatB A1 5–6	5–6	5.5	5.23	444.42		3.25	17.05			288.71	−4.17	0.30
	1805c CatB A1 6–7	6–7	6.5	6.86	1021.17	3.87	3.06	16.27	7.62	7.46	302.04	−3.78	0.30
	1805c CatB A1 7–8	7–8	7.5	5.70	194.45		2.39	13.14			266.00	−4.40	0.30
	1805c CatB A1 8–9	8–9	8.5				2.42	17.02	40.87	1.76	306.94	−4.24	0.44
	1805c CatB A1 9–10	9–10	9.5	6.88	751.46	3.80	2.81	16.32			307.76	−4.62	0.30
	1805c CatB A1 11	11	11.0						11.65	0.88			
SPed*	1805c SPed A5 0	0	0.0						45.56	3.66			

Table 2 (*continued*)

Station	Sample Name	Sediment Depth (cm)	Average Sediment Depth (cm)	Sediment Trace Metal Concentrations			Porewater Trace Metal Concentrations				Authigenic Thallium		
				$[Al]_{bulk}$	$[Mn]_{bulk}$	$[Fe]_{bulk}$	$[Mn]_{pore}$	$[Fe]_{pore}$	$[Tl]_{pore}$	$[Tl]_{error}$	$[Tl]$	$\varepsilon^{205}Tl$	error
				(wt%)	(ppm)	(wt%)	(µM)	(µM)	(pM)	(pM)	(ppb)		(2SD)
	1805c SPed A5 0–1	0–1	0.5	5.19	253.88	4.56	0.05	40.07	60.65	2.40	180.51	−4.63	0.30
	1805c SPed A5 1–2	1–2	1.5	5.76	532.36	5.05	0.07	48.20	42.16	2.04	272.01	−5.20	0.30
	1805c SPed A5 2–3	2–3	2.5	6.21	300.66	3.75	0.10	63.75	57.60	2.97	327.93	−4.88	0.33
	1805c SPed A5 3–4	3–4	3.5	5.78	432.63	3.24	0.11	36.81	28.60	1.17	617.11	−5.10	0.30
	1805c SPed A5 4–5	4–5	4.5	6.55	326.20	3.79	0.15	42.33	53.11	2.76	301.54	−4.78	0.30
	1805c SPed A5 5–6	5–6	5.5	6.43	324.61	3.89	0.14	34.09			548.76	−4.30	0.30
	1805c SPed A5 6–7	6–7	6.5	7.18	598.58	4.15	0.20	50.28	25.60	2.37	290.30	−4.58	0.30
	1805c SPed A5 7–8	7–8	7.5	6.53	336.36	3.96	0.22	39.34			322.11	−4.20	0.48
	1805c SPed A5 8–9	8–9	8.5	6.33	331.11	3.71	0.24	73.83	51.20	4.04	296.00	−4.93	0.45
	1805c SPed A5 9–10	9–10	9.5	5.78	472.23	3.33	0.21	26.47			401.19	−4.52	0.30
	1805c SPed A5 11	11	11.0						9.81	0.51			
Blas*	1805c Blas B3 0	0	0.0						76.74	2.79			
	1805c Blas B3 0–1	0–1	0.5	5.51	108.61	2.10	0.14	70.79	65.08	2.91	215.98	−4.52	0.30
	1805c Blas B3 1–2	1–2	1.5	5.16	289.47	1.94	0.21	62.59	17.89	0.76	223.76	−4.35	0.35
	1805c Blas B3 2–3	2–3	2.5	4.05	60.10	1.44	0.29	59.97	19.21	1.14	98.67	−5.18	0.30
	1805c Blas B3 3–4	3–4	3.5	3.88	228.41	1.23	0.36	58.12			176.11	−4.93	0.48
	1805c Blas B3 4–5	4–5	4.5	5.97	121.89	2.24	0.37	55.61	25.55	1.16	125.96	−4.37	0.30
	1805c Blas B3 5–6	5–6	5.5	4.91	73.92	1.68	0.39	59.84			160.39	−4.14	0.35
	1805c Blas B3 6–7	6–7	6.5	4.98	235.59	1.51	0.44	53.17	30.68	1.58	166.41	−4.26	0.39
	1805c Blas B3 7–8	7–8	7.5	6.36	78.71	2.25	0.42	52.34			188.20	−5.02	0.30
	1805c Blas B3 8–9	8–9	8.5	6.34	82.75	2.28	0.45	43.57	17.77	2.00	195.64	−4.80	0.30
	1805c Blas B3 9–10	9–10	9.5	6.70	286.33	2.00	0.47	41.64			202.81	−4.69	0.30
	1805c Blas B3 11	11	11.0						23.79	0.79			
Sole*	1805c Sole A2 0	0	0.0						75.68	6.01			
	1805c Sole A2 0–1	0–1	0.5						61.77	3.63	256.66	−6.44	0.39
	1805c Sole A2 1–2	1–2	1.5	3.69	298.83	1.83	0.11	28.83	46.94	6.52	257.32	−6.93	0.36
	1805c Sole A2 2–3	2–3	2.5	3.97	357.80	1.96	0.09	12.97	68.11	2.31	278.37	−7.17	0.30
	1805c Sole A2 3–4	3–4	3.5	3.80		0.51	0.07	5.72	56.66	1.99	191.55	−7.31	0.30
	1805c Sole A2 4–5	4–5	4.5	4.22	363.57	2.21	0.06	1.74	33.09	1.87	267.64	−6.37	0.42
	1805c Sole A2 5–6	5–6	5.5	3.93		0.53	0.05	1.45					
	1805c Sole A2 6–7	6–7	6.5	4.08	294.28	1.98	0.04	0.55	21.00	1.41	141.35	−6.46	0.48
	1805c Sole A2 7–8	7–8	7.5	3.84		0.53	0.04	0.51			216.98	−6.47	0.38
	1805c Sole A2 8–9	8–9	8.5	4.31	400.68	2.34	0.02	0.34	22.90	2.10	300.73	−6.54	0.30
	1805c Sole A2 9–10	9–10	9.5	3.79		0.53	0.02	0.29			215.19	−6.15	0.45

Table 2 (*continued*)

Station	Sample Name	Sediment Depth (cm)	Average Sediment Depth (cm)	Sediment Trace Metal Concentrations			Porewater Trace Metal Concentrations				Authigenic Thallium		
				$[Al]_{bulk}$	$[Mn]_{bulk}$	$[Fe]_{bulk}$	$[Mn]_{pore}$	$[Fe]_{pore}$	$[Tl]_{pore}$	$[Tl]_{error}$	$[Tl]$	$\varepsilon^{205}Tl$	error
				(wt%)	(ppm)	(wt%)	(µM)	(µM)	(pM)	(pM)	(ppb)		(2SD)
	1805c Sole A2 11	11	11.0						3.79	0.70			
Peru Margin													
BIGO-05	M77-1 BIGO-05 4–6	4–6	5.0	7.32	414.00	3.40	0.18	15.00			709.45	−7.47	0.30
MUC29	M77-1 MUC29 5–6	5–6	5.5	4.83	203.00	2.07					1547.23	−6.44	0.30
	M77-1 MUC29 8–10	8–10	9.0	5.33	256.00	2.47					711.86	−6.98	0.30
MUC33	M77-1 MUC33 6–8	6–8	7.0	4.50	209.00	1.62	0.05	2.50			330.61	−6.48	0.44
	M77-1 MUC33 10–14	10–14	12.0	4.85	230.00	1.82	0.09	1.00			340.38	−8.17	0.30
MUC21	M77-1 MUC21 6–8	6–8	7.0	7.42	324.00	3.04	0.04	2.50			738.00	−7.14	0.61
	M77-1 MUC21 10–12	10–12	11.0	6.88	317.00	3.07	0.06	1.00			727.69	−6.32	0.38
MUC25	M77-1 MUC25 6–8	6–8	7.0	3.87	223.00	1.55	0.02	11.50			128.73	−7.50	0.33
	M77-1 MUC25 10–12	10–12	11.0	4.03	230.00	1.60	0.02	8.00			84.87	−6.66	0.30
MUC15	M77-1 MUC15 1–2	1–2	1.5	4.14	218.00	2.33	0.09	0.01			193.36	−6.68	0.30
	M77-1 MUC15 4–5	4–5	4.5	4.29	212.00	2.75	0.12	9.00			319.05	−6.76	0.30
MUC27	M77-1 MUC27 2–5	2–5	3.5	5.86	314.00	2.31					131.31	−6.94	0.45

All sediment concentrations are in ratios by mass.

* Blas=San Blas Basin, CatB=Catalina Basin, Patt=Patton Escarpment, SClm=San Clemente Basin, Sole=Soledad Basin, SPed=San Pedro Basin.

3. Results

It should be noted that ratios of bulk sediment trace metal to Al can be utilized to constrain enrichments compared to sedimentation, but due to little deviation in Al ($\pm$ <1 wt%) except for a small number of samples in which this ratio makes no notable difference in trends, this metal/Al ratio has not been employed for interpretive purposes (Table 2). All samples are based on depth (in cm) rather than stratigraphic time, and as such, cannot be directly correlated between sites. The Tl concentrations and isotopes in the lithogenic (non-leached) fraction ($\varepsilon^{205}Tl_{lith}$) of all samples were measured along with Fe speciation of the samples (Supplemental Methods and Supplemental Table 2). Errors for most analyses are too low to list (<2 %), except for Tl isotope values and Tl porewater concentrations, which have errors included.

Based on bottom water oxygen content, Patton Escarpment and San Clemente Basin (Fig. 2) are the most oxic sites (Tyson and Pearson, 1991). The sediment Mn concentrations are generally higher at these sites compared to the others, and are greater than UCC of 600 ppm for Mn (Mclennan, 2001). These concentrations trend towards higher values up the core towards the sediment surface, with an opposite trend in porewater Mn concentrations where concentrations increase downcore. Meanwhile for Fe, the sedimentary values are higher than UCC values of 3.5 wt% (Mclennan, 2001) and remain consistent downcore

except for at 4 cm at Patton Escarpment where there is a large increase to 8 wt% from 4.5 wt%, while porewater Fe concentrations are near non-detectable at these depths. Solid phase authigenic Tl concentrations are similar to previous work (Owens et al., 2017; Chen et al., 2021; Wang et al., 2022) and the other sites in this study and show little downcore variation except for a rapid drop in the top few centimeters of Patton Escarpment from 800 to 400 ppm related to increase of Mn in the porewater. Of the two sites, only San Clemente had porewater Tl concentrations, which are elevated compared to the other sites with a notable increase in porewater concentrations specifically around 3 cm depth (see Supplementary Discussion), which is at approximately the inflection point for both sedimentary and porewater Mn concentrations. Both sections show more positive $\varepsilon^{205}Tl_{auth}$ values near the core tops, with a decreasing trend down core. Patton Escarpment shows a stepwise decrease downcore, with sudden shifts at 3–4 cm and 6–7 cm, while San Clemente is more gradual but also has a slight rise in isotope composition (~1 ε unit) at approximately 9 cm.

The remaining cores have lower bottom water oxygen values than San Clemente and Patton Escarpment (Fig. 3). These cores also maintain low Mn concentrations (<1000 ppm), lower Fe concentrations than the oxic sites (<4.5 wt%), consistent but low authigenic Tl concentrations (mostly <400 ppb), and consistent and very low porewater Tl concentrations (~50 pM), hence the Tl concentrations are not displayed in
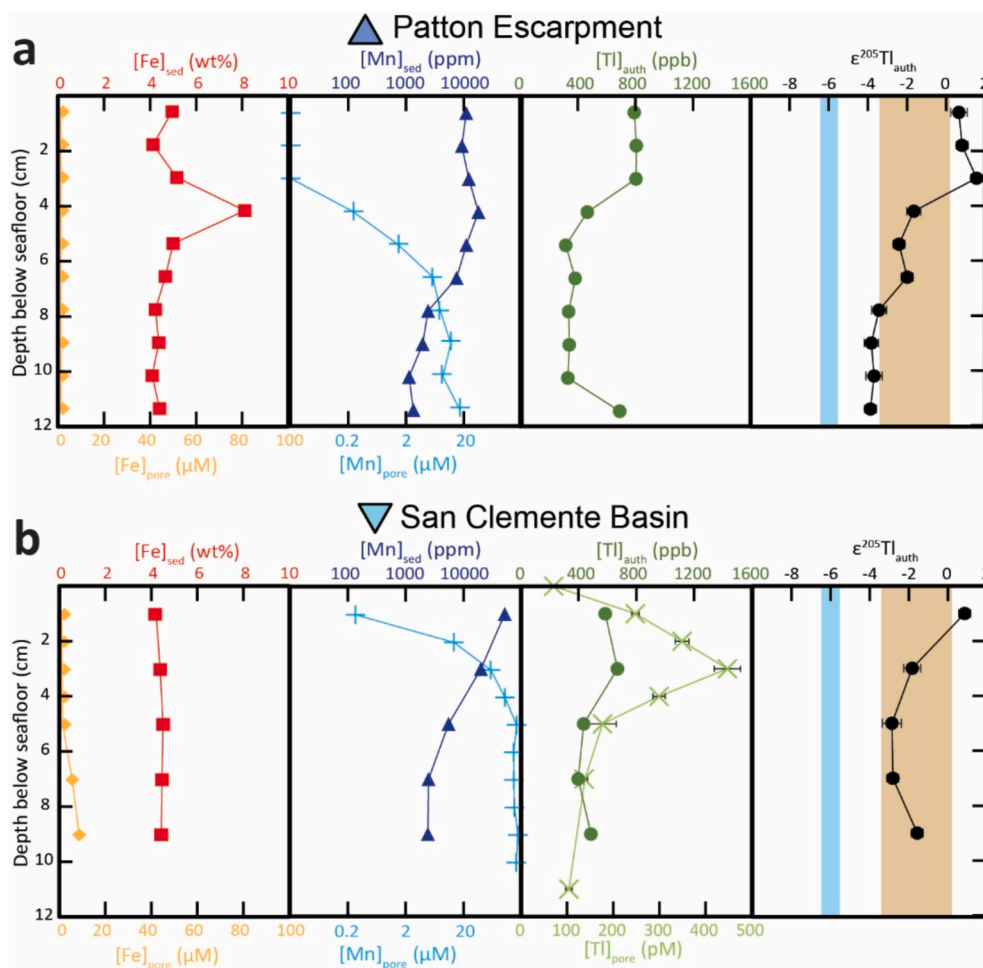
Fig. 2. Geochemical stratigraphic columns of the sediments at the most oxic sites Patton Escarpment (a) and San Clemente Basin (b). The geochemical data includes Fe concentrations (sediments are red squares; porewaters are orange diamonds), Mn concentrations (sediments are dark blue triangles; porewaters are light blue pluses), Tl concentrations (sediments are dark green circles; porewaters are light green crosses), and Tl isotopes (black circles). Errors on thallium isotopes and thallium porewater concentrations are 2σ, minimum of 0.3 ε units for isotopic values. The Mn concentrations are on a logarithmic axis for ease of comparison among the large range of concentrations. For all concentration data, the upper axis is for sediments and lower axis is for porewaters. Typical range for oxic seawater (blue) and source values (brown) are highlighted boxes on the Tl isotope plots based on previously determined flux and reservoir compositions (Rehkämper et al., 2002; Nielsen et al., 2006c, 2017; Owens et al., 2017; Owens, 2019).

Fig. 3 (Supplemental Figs. 1–5). Three sites (Fig. 3a-c), Catalina Basin, San Pedro Basin, and San Blas Basin, all have elevated porewater Mn (>0.1 μM) and Fe (>10 μM) concentrations throughout most of the sediment core. Of these sites, Catalina Basin, the site with the highest bottom water oxygen content, shows an increasing trend in the porewater Fe concentrations from 0 μM to 20 μM. San Blas shows the opposite trend of decreasing porewater Fe concentrations, from 80 μM to 40 μM. The other trend in this data is an increase in porewater Mn concentrations in San Pedro and San Blas Basins, from 0.05 μM to 0.21 μM and 0.15 μM to 0.45 μM, respectively. In terms of $\varepsilon^{205}Tl_{auth}$, these sites all average around −4.5, with little deviation among samples and little change downcore, which results in more positive than typical seawater values ($\varepsilon^{205}Tl = -6.0 \pm 0.4$) and more negative than source values ($\varepsilon^{205}Tl = -1.8 \pm 1.9$). The majority of Soledad Basin and Peru Margin (Fig. 3d and e) samples have lower porewater Mn (<0.1 μM) and Fe (<10 μM) concentrations than the other reduced sites. At Soledad, there is a decrease in both porewater Mn and Fe downcore, starting at 0.11 μM and 30 μM, respectively, in the top layer to lower values at deeper depths. As Peru represents different depths in various sites across a transect, downcore variation in geochemical constituents relevant to Tl isotopes cannot be determined. Soledad and Peru have $\varepsilon^{205}Tl_{auth}$ values of ~−6.8, near seawater composition or slightly more negative,

with little downcore variation.

4. Discussion

4.1. Thallium isotopes under various sedimentary redox states

4.1.1. Geochemical differentiation of sites

The redox conditions for all these localities yield a wide range of Tl isotopic compositions. Few are similar to the lithogenic isotopic compositions (Supplemental Fig. 1), which are near expected values for continental source material with minimal variation, indicating accurate leaching of the authigenic material. The Tl data primarily coalesce around three groupings (Fig. 4), two sites with values at or above sources to the ocean (−1.8 ± 3.8), three sites that have lower but more intermediate isotopic compositions (−4.5 ± 0.8), and one site plus a transect that have values around a seawater signature (−6.8 ± 1.0). The most positive Tl isotopes localities are the oxic stations at Patton Escarpment and San Clemente Basin (Fig. 2), which have elevated Mn and Fe concentrations in the surface sediments reflective of ferromanganese mineral formation (Rue et al., 1994; Algeo and Maynard, 2004; Tribovillard et al., 2006). Based on their high Mn concentrations and the Wang et al. (2022) 'decision tree', these upper sediments in the oxic
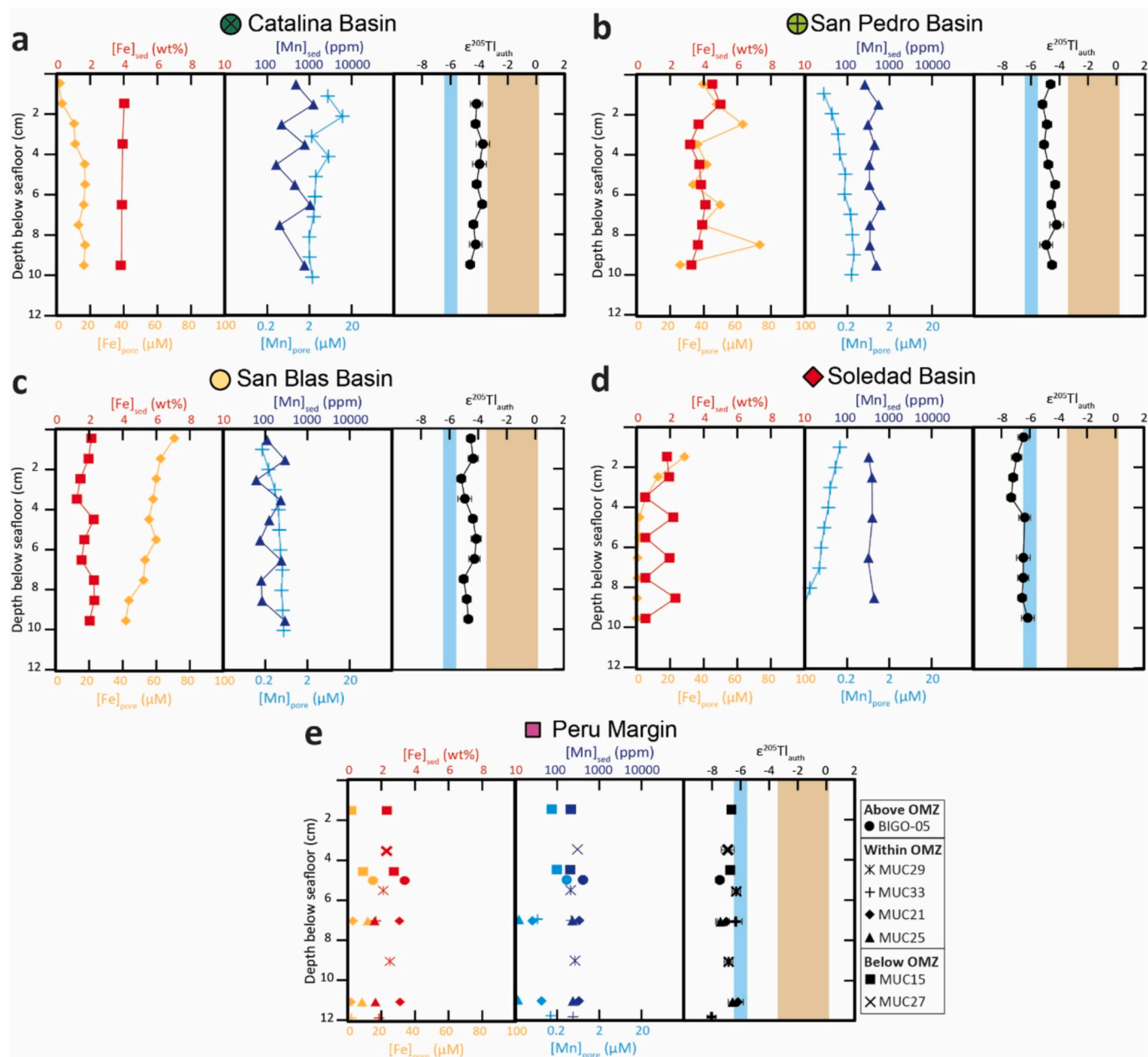
Fig. 3. Geochemical stratigraphic columns of the sediments at the reducing sites Catalina Basin (a), San Pedro Basin (b), San Blas Basin (c), Soledad Basin (d), and the Peru Margin (e). The geochemical data includes Fe sediment (red squares) and porewater concentrations (orange diamonds), Mn sediment (dark blue triangles) and porewater concentrations (light blue pluses), and Tl isotopes (black circles). Peru Margin data utilizes shapes based on exact locality rather than data type, but color matches previous sites' data type. Errors on thallium isotopes and thallium porewater concentrations are 2σ, minimum of 0.3 ε units for isotopic values. The Mn concentrations are on a logarithmic axis for ease of comparison among the large range of concentrations. Typical range for oxic seawater (blue) and source values (brown) are highlighted boxes on the Tl isotope plots based on previously determined flux and reservoir compositions (Rehkämper et al., 2002; Nielsen et al., 2006c, 2017; Owens et al., 2017; Owens, 2019).

sections are not recording seawater values (Supplemental Table 2). Downcore sediments are more ambiguous with regard to the 'decision tree' because the lack of barium (Ba) concentrations makes it hard to precisely determine where these samples lie on the decision tree. On the other hand, the most negative sites, Soledad Basin and the Peru Margin (Fig. 3d-e), have no detectable bottom water oxygen contents with low concentrations of Mn and Fe, which place these sites as anoxic. Similarly, when sorted by the Wang et al. (2022) decision tree, these samples are most probably able to accurately record seawater values based on low Mn and high U contents (Supplemental Table 2).

However, the remaining three sites, Catalina Basin, San Pedro Basin, and San Blas Basin, are more difficult to classify (Fig. 3a–c), with various

intermediate geochemical compositions between the oxic and anoxic sites while also recording Tl isotopic values between seawater and sources, leading to the broad categorization as 'suboxic'. This classification is in opposition to Wang et al. (2022)'s decision tree, which would suggest these samples are likely to record seawater values due to low Mn and high U contents (Supplemental Table 2), indicating they should be similar to other anoxic sites rather than isotopically distinct. These three intermediate sites generally have the most transitional bottom water oxygen content of these sites (0.1–20 μM O$_2$), though all three are closer to or fully within the anoxic definitions (Reimers et al., 1986; Leslie et al., 1990; Berelson et al., 2005; Chong et al., 2012). All have low sedimentary Mn concentrations with some samples having
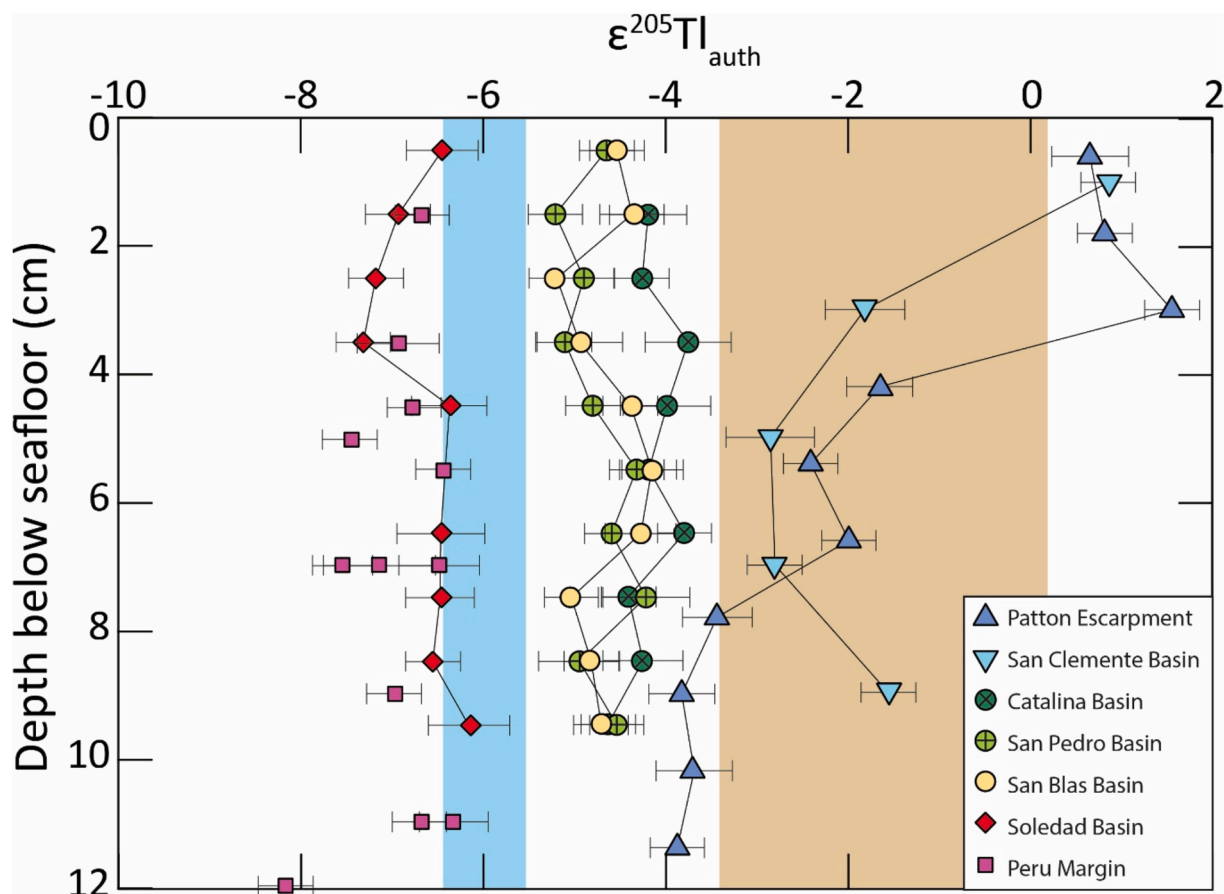
Fig. 4. Full range of Tl isotopes for all sites studied, with shapes and colors matching Fig. 1. Note that oxic sites are blue triangles, 'suboxic' are yellow to green circles, and anoxic are red to purple squares and diamonds. Errors on thallium isotopes are 2σ, minimum of 0.3 ε units. Typical range for oxic seawater (blue) and values (brown) are highlighted boxes on the Tl isotope plots based on previously determined flux and reservoir compositions (Rehkämper et al., 2002; Nielsen et al., 2006c, 2017; Owens et al., 2017; Owens, 2019).

elevated Fe concentrations, but mostly less than the oxic sites. In all three sites, the porewater Mn concentrations are between those found downcore in the oxic sediments and the porewaters of the anoxic sediments while the porewater Fe concentrations are higher than all other sites. These porewater concentrations would suggest that these sites are partially in the manganous zone though primarily ferruginous, with Catalina Basin more manganous and San Pedro and San Blas Basins more ferruginous; further referrals to these 'suboxic' samples will henceforth be as manganous-ferruginous when directly referencing the samples. There are some small increases in hydrogen sulfide and decreases in sulfate (Berelson et al., 1987, 2005; Leslie et al., 1990), though these are not persistent enough to indicate fully anoxic conditions. As previous discussions on the Tl isotope mass balance utilizes the suboxic nomenclature (Nielsen et al., 2011; Owens, 2019) and these samples primarily align in Tl isotope values (Fig. 4), these manganous-ferruginous sediments will be considered suboxic when discussing the mass balance in broader terms below as well as for implications on deep-time interpretations where the differentiation of the various 'suboxic' regimes is harder to quantify.

Importantly, these three broad classifications of bottom water redox conditions document Tl isotope variation. The endmember values from oxic and anoxic sites broadly fall within the expected values based on previous work (Nielsen et al., 2011, 2013, 2017; Owens et al., 2017) and mass balance averages. Additionally, these two classifications are likely controlled by local Mn oxides driving Tl isotope values more positive at oxic sites and low Mn oxides with high pyrite formation capturing seawater values at permanently anoxic locations. These follow expectations and the decision tree for Mn and U concentrations (Wang et al.,

2022), but Ba contents are not known for this work to definitively follow this line of reasoning. However, the manganous-ferruginous sites have low Mn and elevated U, with the Tl isotopes having values that do not match the typical anoxic values. Thus, the decision tree (Wang et al., 2022) provides a false positive for these settings, where samples that should record seawater based on the decision tree do not record seawater isotopic compositions.

4.1.2. Thallium isotopes from oxic sediments

Patton Escarpment (Fig. 2a) and San Clemente Basin (Fig. 2b) represent the most oxic sites of the California-Mexico Margin. The most positive values in Tl isotopes through this study are found in the shallowest sediments near the sediment–water interface. These samples are positive with an average of (+1.0), which is greater than the typical marine input values (~−1.8) (Owens, 2019), and therefore more positive than the lithogenic component of these samples of ~−2.6 (Supplemental Fig. 1). Such a $\varepsilon^{205}Tl_{auth}$ value is likely caused by the influence of Mn oxides, due to their positive isotope composition (Rehkämper et al., 2002; Rehkämper and Nielsen, 2004; Nielsen et al., 2009). However, the fact that these samples are not expressing the full positive values that are known from Mn oxides (~+5.3 to +14.8) indicates that only a portion of the captured isotope signature is from Mn oxides, suggesting there is a mixed-origin signal or that diagenetically altered Mn oxides are being incorporated (Rehkämper et al., 2002). The concentration of Tl is higher in the authigenic fraction than the lithogenic fraction, the latter of which records typical marine input values, indicating detrital material is unlikely to be incorporated into the authigenic leach in order to drive these isotopic compositions
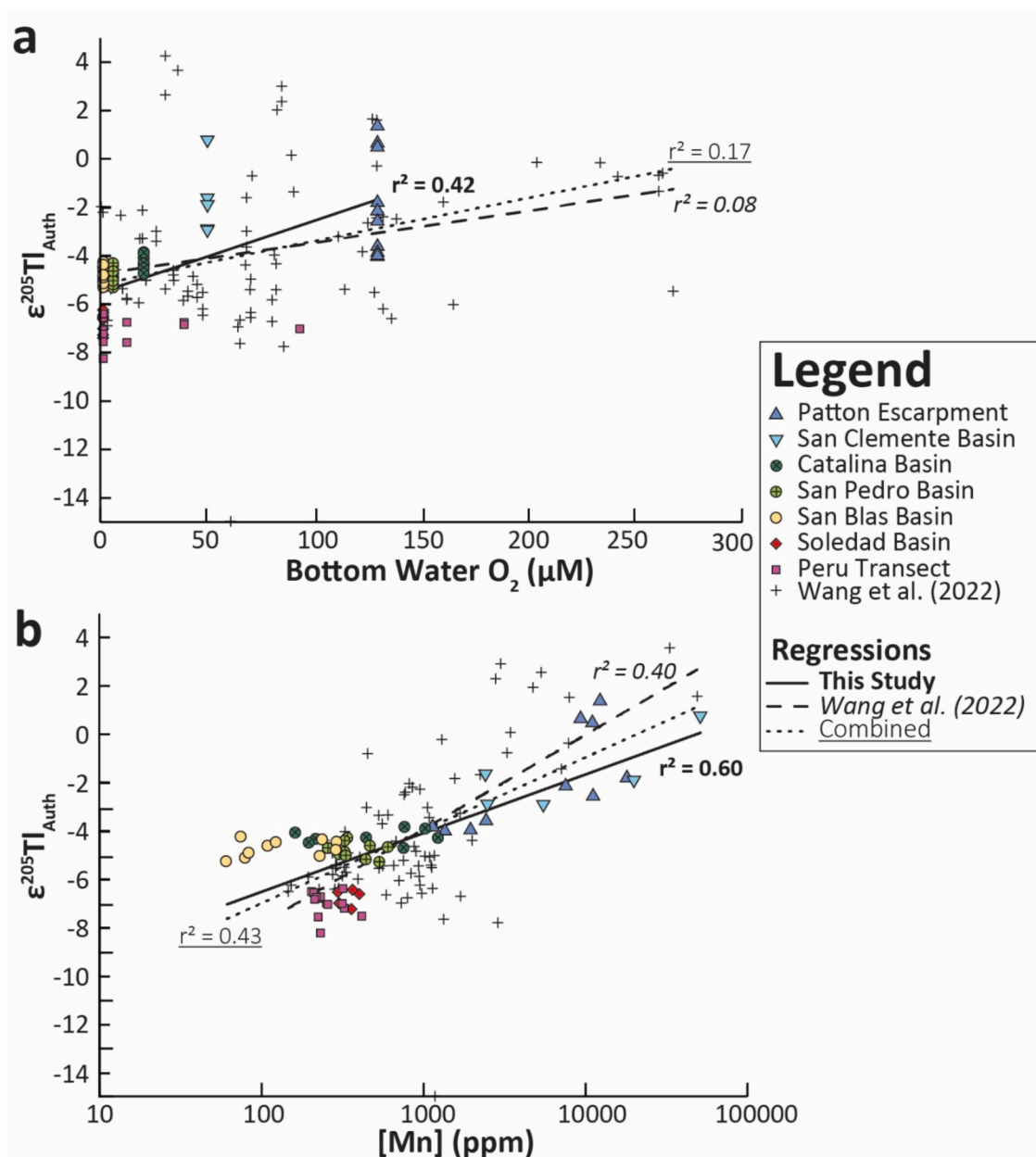
Fig. 5. Comparison of Tl isotopic compositions to bottom water O_2 (a) and Mn oxides as represented by sediment Mn concentrations (b). Data from all measured samples are included, with additional data from Wang et al. (2022), divided up by color and shape to match Fig. 1. Note that oxic sites are blue triangles, 'suboxic' are yellow to green circles, and anoxic are red to purple squares and diamonds. Linear regressions were applied to the bottom water oxygen content and logarithmic regression to Mn concentrations, including just those for this study (straight line, bolded regression), Wang et al. (2022)'s dataset (long dashed line, italicized regression), and combined (short dashed line, underlined regression). Mn concentrations are on a logarithmic scale to effectively show range of values. Errors for Tl isotopes were excluded due to relatively low 2σ across samples measured and improved ease of discerning samples.

(Supplemental Fig. 1).

The possible cause of the mixed isotopic composition of the upper oxic sediments (ε^{205}Tl = −2.0 to +2.0) cannot be directly determined due to limited research into authigenic compounds under oxic marine settings beyond solely Mn oxides in the form of birnessite, especially compared to the isotopic variability of downcore sediments. Assuming a basic mass balance mixing using end members of seawater isotopic values, e.g., pyrite with limited or no isotopic fractionation from seawater (Owens et al., 2017), and Mn oxides (Rehkämper et al., 2002; Rehkämper and Nielsen, 2004; Nielsen et al., 2006b), the isotope values of the shallowest oxic sediments suggest between 39 % and 69 % of the isotopic signal is from Mn oxide averaging ~54 %, with the remaining from pyrite with no fractionation of seawater values. It is possible that

there could be a negative fractionation due to the incorporation of organic matter fractionated Tl (Ostrander et al., 2025), but the relatively low TOC of this site (~1 wt% TOC) indicates that organic matter also is unlikely to drive this fractionation (Bruggmann et al., 2023). The range of values for the estimated mixed composition is due to the large natural variation of known Tl isotopic values for Mn oxides, which is between + 5.3 and + 14.8 epsilon units (Rehkämper et al., 2002; Nielsen et al., 2004, 2009). But these calculations show that the oxic sedimentary Tl isotopic signature is primarily controlled by Mn oxides for much of these shallow Mn-rich sediments. Nevertheless, as it is not possible for the isotopic composition to be composed of only Mn oxides and the oxic nature of these sediments limit pyrite formation (Supplemental Fig. 2), there may be a secondary authigenic phase contributing to the isotopic

value. Such authigenic phases may be clays that are known to incorporate potassium that is readily replaced with Tl in other systems (Rader et al., 2019; Olesen et al., 2025), another Mn oxide other than birnessite that has been documented to have a smaller fractionation from seawater (Phillips et al., 2023), or potentially organic matter that may induce a minor isotope fractionation from seawater (Ostrander et al., 2025). However, these alternatives are not fully constrained in modern marine systems as this was from a non-marine system (see Supplemental Discussion).

Continuing downcore in these two oxic sites, there is a trend towards more negative isotope values from $+1.0$ to ~-2.0 or even more negative values. Patton Escarpment's $\varepsilon^{205}Tl_{auth}$ values exhibit another small negative shift deeper in the core, with these deeper samples having more negative compositions than the seawater input values. It should be noted that there is an increase in porewater Mn at the depth of the upper Tl isotopic shift at the Patton Escarpment site, along with a decrease in authigenic Tl, while the lower negative shift in Tl isotopic composition occurs with a decrease in solid Mn concentrations. At San Clemente Basin, there are decreasing solid phase Mn concentrations that align with the decreasing $\varepsilon^{205}Tl_{auth}$ values. A notable increase in Tl porewater concentrations also occurs at San Clemente Basin with the change in $\varepsilon^{205}Tl_{auth}$ towards more negative values, coinciding with an increase in porewater Mn concentrations downcore. These negative shifts suggest a close relationship between the Mn composition of the sediment and the Tl isotopic signature, where dissolution of solid phase Mn removes some of the Mn oxide isotopic signature in the sedimentary $\varepsilon^{205}Tl_{auth}$, causing the values to become more negative. Other sedimentary factors, such as the authigenic phases previously mentioned, must also influence these values as these isotopic compositions fall far below typical Mn oxide $\varepsilon^{205}Tl$ compositions. A more detailed study into porewater Tl isotopes and concentrations may provide a better understanding of the isotopic changes measured, specifically the impact of downcore redox conditions and/or Mn concentrations on the Tl isotopic compositions within such sediments. However, such a study requires a significant quantity (>500 ml) of pore fluids to measure isotopes, which was not possible during this work. The issue is further compounded when interpreting the porewater Tl concentrations by potentially non-ideal methods utilized when using rhizons aboard the R/V Oceanus (see Supplemental Discussion).

Importantly, all $\varepsilon^{205}Tl_{auth}$ values determined for these two sites are more positive than nearly all samples from other sites, as is expected based on the limited to nonexistent pyrite formation for incorporation of Tl with a seawater isotopic signature along with the presence of isotopically more positive Tl in Mn oxides. This pattern maintains the limited utility of oxic sediments as a record for the seawater Tl isotope value.

4.1.3. Thallium isotopes in suboxic sediments

The sites that would be considered 'suboxic' due to factors such as low but detectable oxygen in two of the three sections and elevated Fe and Mn in the pore waters, which were discussed above and therefore make these manganous-ferruginous show a more mixed Tl isotopic signature. Catalina Basin (Fig. 3a), San Pedro Basin (Fig. 3b), and San Blas Basin (Fig. 3c) have generally similar Tl isotope signatures (Fig. 4) that are more positive (-4.5 average) than the average global oxic seawater value of -6.0 but more negative than the typical marine input values ($\sim$-1.8). Since these values are more positive than typical seawater, the values indicate either incomplete adsorption of Tl onto the very limited amount of pyrite that formed or a mixed signal with other Tl-containing phases. However, non-quantitative Tl values in pyrite has been shown to have minor, if any, fractionation in a small redox stratified pond (Ostrander et al., 2023). Instead, the cause of the mixed signal might be similar to the more oxic sediments, but this speculation is difficult to verify. Specifically, sedimentary Mn concentrations are considered low enough in all samples to not be a major contributing component (Wang et al., 2022). Meanwhile, the pyrite contents are lower in these sediments through the core (Supplemental Fig. 3),

indicating that the bottom water redox conditions are more reducing but the seawater values may only be partially incorporated into the signal and are unlikely the major contributor to the overall Tl signature. Basic mass balance such as done for the oxic sediments suggest between 5 % and 21 % of the signal is from Mn oxide inclusion, averaging $\sim$ 11 %. Under any of these circumstances, there could be the potential for minor inclusion of Mn oxides in the sedimentary Tl isotopic values with a larger portion being associated with pyrite or other seawater-preserving authigenic phase. It is also possible that the process of pyrite formation is capturing the highly fractionated Tl values of Mn oxides that are undergoing reduction, thus requiring the dissolution of Mn oxides and pyrite formation to occur in close proximity. This process, if it was occurring, could skew the isotopic composition of just the pyrite without having Mn oxide present in the sediments, which could be a possibility considering the low Mn concentrations in these manganous-ferruginous sediments and potential for Mn remobilization at these sites (McManus et al., 2012). One last possibility is that the sedimentation rates of these sites allow for a more extensive redox gradient within the sediments. Such a gradient could allow for greater intermingling of isotopic signatures than the core tops of other studies alone (see Supplemental Discussion).

In addition, based on the relative stability downcore across all three sites, it is reasonable to assume that the isotopic signature is preserved and unaltered from near the sediment surface under even mildly reducing conditions, with little measurable alteration after burial. This downcore stability may be due to consistent benthic redox conditions creating the same isotopic signatures or due to the preservation of the Tl isotopes adsorbed to authigenic phases as geochemical conditions change downcore. As there is minimal change in the other geochemical tracers utilized for this study, it is difficult to differentiate between these two ideas, at least compared to the more mineralogically influenced oxic sediments, though Mn remobilization in adjacent regions (McManus et al., 2012) points towards the latter. Nevertheless, Tl isotope preservation of sedimentary isotopic composition through early diagenesis appears to be generally robust under at least mildly reducing environments.

4.1.4. Thallium isotopes in anoxic sediments

Soledad Basin in the California-Mexico Margin (Fig. 3d) represents a perennially anoxic environment, which has very low Mn and Fe concentrations in both sediment and porewaters (Bruggmann et al., 2023). The Tl isotope records for this section are similar to what would be expected for other anoxic to euxinic basins, recording near-seawater isotopic values (Owens et al., 2017; Fan et al., 2020; Wang et al., 2022; Ostrander et al., 2024). This section confirms that these permanently anoxic settings record overlying seawater isotopic values due to adsorption onto pyrite based on increased sulfide content (Berelson et al., 2005; Chong et al., 2012) and pyrite-enriched sediments (Supplemental Table 2). Therefore, based on these sections it is possible that any anoxic sediment can reproduce seawater values as long as there is limited Mn oxide cycling (Wang et al., 2022) with pyrite formation. However, a noticeable increase in sulfide content (Fan et al., 2020) seems necessary to allow for meaningful pyrite formation (Hardisty et al., 2018). Other pertinent redox factors, such as low oxygen based on U enrichments and high productivity based on Ba enrichments and total organic carbon content, may also be useful in prescribing sediments in which seawater values can be faithfully captured beyond elevated pyrite content (Wang et al., 2022). Similar to the manganous-ferruginous sites, values at Soledad Basin also maintain consistent isotopic composition downcore compared to the oxic sites, supporting the thesis that isotopic values are unaffected by downcore changes and remain consistent through early diagenesis when porewaters are reducing.

The Peru Margin sites cover a range of bottom water conditions across the oxygen minimum zone (OMZ), but almost all sites within or above the Peru OMZ have a bottom water oxygen content that is below the detection limits of the analytical methods and those below the OMZ
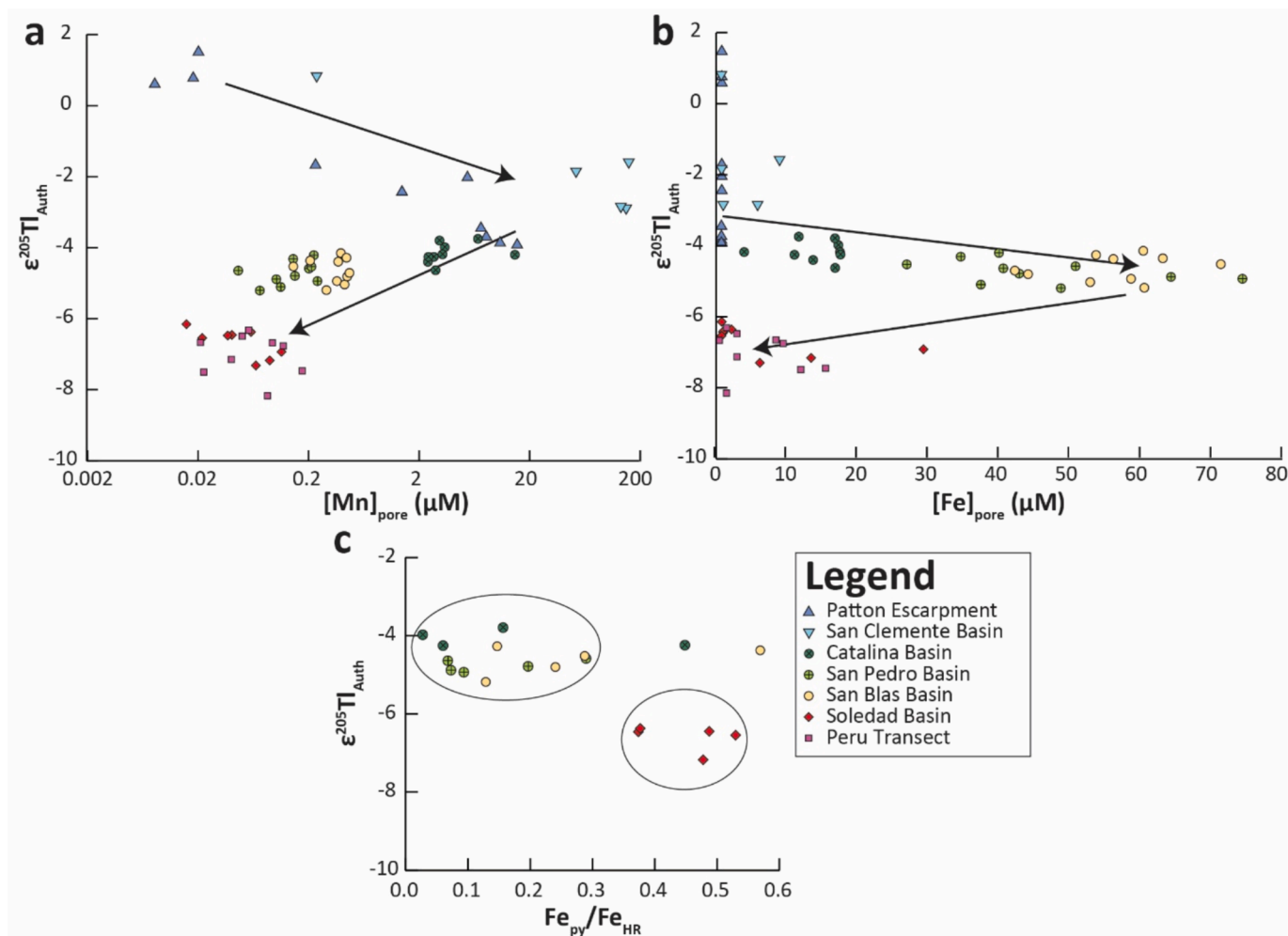
Fig. 6. Comparison of Tl isotopic compositions to porewater Mn concentrations as a representation of manganous conditions (a), porewater Fe concentrations as a representation of ferruginous conditions (b), and Fe_{py}/Fe_{HR} ratios (see Supplemental Methods) to indicate sulfidic conditions and formation of pyrite (c). Data from all measured samples are included, divided up by color and shape to match Fig. 1. Note that oxic sites are blue triangles, 'suboxic' are yellow to green circles, and anoxic are red to purple squares and diamonds. General trends of data in (a) and (b) are shown with arrows, while the two clusters of data when working with Fe_{py}/Fe_{HR} are shown in (c). Errors for Tl isotopes were excluded due to relatively low 2σ across samples measured and improved ease of discerning samples.

with higher bottom water oxygen have a similar local geochemical signature to the rest of the Peru Margin (Böning et al., 2004; Scholz et al., 2011; Noffke et al., 2012). Along with these geochemical signatures, the Mn contents of the Peru Margin are similar to Soledad Basin, indicating that this transect primarily represents another anoxic setting. All the Tl isotope values match those of other anoxic to sulfidic sites published to date (Owens et al., 2017; Fan et al., 2020; Wang et al., 2022), having similar or even more negative $\varepsilon^{205}Tl_{auth}$ values to seawater (Fig. 3e). Even the deepest and furthest site from the Peru OMZ, which has more bottom water oxygen (MUC27 with 93.4 μM dissolved O_2 at 2025 m depth), maintains the same Tl isotope signature as any previously described anoxic sample, which may be due to having similar porewater redox conditions as all other measured anoxic sections, as seen in Mn and Fe sediment and porewater concentrations (Scholz et al., 2011, 2014a), even with overlying oxygen (Owens et al., 2017; Fan et al., 2020; Wang et al., 2022). This situation may suggest that reducing porewaters might be most important for the Tl isotope signature rather than overlying water conditions. Alternatively, these deeper sites may have mixed material from shallower sections as evidenced in other geochemical signatures (Scholz et al., 2024). Both Soledad Basin and the Peru Margin effectively fit expectations to record seawater values based on the decision tree of Wang et al. (2022), indicating only specific settings create false positives such as the

manganous-ferruginous sediments.

4.2. Refinement of the reducing sinks for thallium isotopes

4.2.1. Factors affecting the thallium isotopic signature of all sections

Notably, there are two primary non-silicate phases that Tl has traditionally been associated with in marginal marine sediments, Mn oxides and pyrite (Owens et al., 2017; Nielsen et al., 2017; Owens, 2019; Wang et al., 2022; Ostrander et al., 2023), though other factors, such as anoxia (U enrichment) and productivity (Ba enrichment and TOC) may also need to be considered in the preservation potential of sediments (Wang et al., 2022; Ostrander et al., 2025; Olesen et al., 2025). Broadly, there is some correlation between bottom water oxygen content and the $\varepsilon^{205}Tl_{auth}$ value of the sediments (Fig. 5a). This correlation shows a general relationship between the redox state of the water column and the isotopic composition, with a relatively low but non-incidental r^2 value of 0.42. This relationship is notably better than the broader range of data from Wang et al. (2022), likely due to the smaller number of sites included. Combining the two provides a poor correlation (r^2 value of 0.17), indicating oxygen content may play a small part of the composition of the samples.

Sedimentary Mn concentrations, which is likely the primary driver of the above generalized relationship with bottom water oxygen, show a

moderate correlation to the $\varepsilon^{205}Tl_{auth}$ (Fig. 5b) when all data is compared from this study, with an r^2 value of 0.60 for a logarithmic regression (Supplemental Fig. 6). This is slightly greater than correlations found between Mn content and $\varepsilon^{205}Tl_{auth}$ from Wang et al. (2022) of $r^2 = 0.40$, and when combined averages to $r^2 = 0.43$. In both studies, the more oxic settings with higher Mn content tend to be a greater control on the Tl isotopic composition, indicating the expected effect of Mn oxides. Of important note is that the manganous-ferruginous sediments and anoxic sediments of this study, though distinct in Tl isotopic values, have similarly low Mn content, with no correlation between sedimentary Mn concentrations and $\varepsilon^{205}Tl_{auth}$ (Supplemental Discussion, $r^2 = 0.01$). Therefore, there are greater controls on these low-oxygen sediments than just potential Mn oxide inclusion that must be accounted for to explain the division between these two sedimentary redox states' effects on Tl isotopes.

Additional comparisons can be seen when cross-plotting the porewater Mn and Fe concentrations with the $\varepsilon^{205}Tl_{auth}$ values of these sediments (Fig. 6a and b). For Mn, there are low concentrations in oxic sediments that increase downcore with decreasing Tl isotopic values, reaching the peak concentrations in the lower oxic sections. The Mn concentrations then transition back towards lower values as bottom water oxygen content decreases along with a continuing negative shift in $\varepsilon^{205}Tl_{auth}$. The manganous-ferruginous sites sit in this transition. Their porewater Mn concentrations are not as high as the oxic settings at depth, though the upper oxic sediments do also have low porewater Mn due to the precipitation of Mn as Mn oxides. But the manganous-ferruginous sediments also are not as low as most of the anoxic settings where Mn cannot accumulate in porewaters due to overlying low-oxygen conditions. The $\varepsilon^{205}Tl_{auth}$ values follow the trend with decreasing porewater Mn also having decreasing Tl isotopic compositions (Fig. 6a). A similar relation occurs for Fe but with the manganous-ferruginous sites having the highest concentrations (Fig. 6b) instead of the oxic sections (Fig. 6b). These trends show, for both Fe and Mn porewaters, there are stepwise changes in $\varepsilon^{205}Tl_{auth}$ as the samples progress toward reducing conditions, which are offset based on the redox potential of Fe and Mn. These steps partially explain the distinct grouping of the Tl data (Fig. 4), with the transitional phases between oxic and anoxic inducing intermediate Tl isotopic values in the sediments.

This stepwise change can be further expounded upon by considering Fe speciation, which is a means to differentiate the reactivity of Fe based on the water column redox state (see Supplemental Methods), an often necessary tool for determination of ancient local redox conditions (Hardisty et al., 2018). Specifically, Fe speciation can differentiate between the ferruginous and sulfidic samples through the ratio of pyritic Fe (Fe_{py}) and highly reactive Fe (Fe_{HR}), with higher ratios between the two indicating a more sulfidic state (Poulton and Canfield, 2011; Hardisty et al., 2018; Raiswell et al., 2018). As sulfide content is not fully available for all sites and depths (Berelson et al., 1987, 2005; Leslie et al., 1990; Böning et al., 2004; Scholz et al., 2011; Chong et al., 2012; Noffke et al., 2012), the Fe_{py}/Fe_{HR} has been utilized as a proxy for the California-Mexico Margin sulfide content in the sediments and formation of pyrite. There is a clear clustering of the manganous-ferruginous sites at higher $\varepsilon^{205}Tl_{auth}$ values and lower Fe_{py}/Fe_{HR} ratios. Meanwhile, Soledad Basin represents the more anoxic state with raised sulfide content and a more negative $\varepsilon^{205}Tl_{auth}$ with higher Fe_{py}/Fe_{HR} (Fig. 6c). With a few minor exceptions, this relation provides a relative minimum pyrite composition necessary to accurately record seawater values, with all Soledad samples having at least Fe_{py}/Fe_{HR} of 0.35. This ratio indicates that raised sulfide content is another important factor beyond just anoxic sediments (Fan et al., 2020; Wang et al., 2022), a feature that extends to the Peru Margin at large (Böning et al., 2004; Scholz et al., 2011, 2014a; Noffke et al., 2012).

4.2.2. Refining the low oxygen sinks

Due to the range of chemical conditions that occur within suboxia,

there has previously been limited analysis of Tl isotopic signatures under suboxic conditions, with only a couple of data points covering a large isotopic range (−6.0 to 0.0) prior to this study (Rehkämper et al., 2004; Nielsen et al., 2011; Owens, 2019). More recent data may fill in some of the data gaps, though not classified as such (Wang et al., 2022). Still, there are several additional constraints this study provides for low oxygen sinks for the Tl isotopic system. The 'suboxic' sections, specifically manganous-ferruginous as defined in this study, have values between −3.7 to −5.2, averaging −4.5. These seem to provide a far more reasonable conservative range and average isotopic composition for the suboxic sink in the modern, indicating that manganous-ferruginous conditions have a narrow and consistent 1.5 ε unit range offset from the anoxic seawater values.

In addition, the anoxic to sulfidic sink remains the same as previous work suggests (Nielsen et al., 2011; Owens et al., 2017; Fan et al., 2020; Wang et al., 2022; Ostrander et al., 2023, 2024). The range of $\varepsilon^{205}Tl_{auth}$ data present at Soledad Basin and the Peru Margin all are within a range that encompasses seawater composition (see Supplemental Discussion). This conclusion further supports that this sink is ideal for recording seawater composition in deep time.

These results suggest that both low oxygen sinks can be utilized for recording seawater isotopic compositions in deep time. The anoxic to euxinic sediments are able to record a seawater isotopic composition without notable fractionation from seawater. Therefore, it is reasonable to identify these sediments as an archive to accurately reconstruct ancient seawater composition. Of interest to this study, the suboxic sediments may also be effective at recording oceanic compositions but with an isotopic fractionation or offset from original seawater values. These sediments represent Tl isotopic signatures that at the midpoint between oxic seawater compositions and source values. Therefore, if geochemical proxies can identify that ancient sediments are potentially within the broad range of suboxic conditions, these sediments may provide a Tl record but with a diminished range of seawater composition. The range of values would be smaller, only reaching −4.0 to −2.0 rather than the full range of −6.0 to −2.0 from anoxic to euxinic sediments. Thus, a muted signal would likely exist in these suboxic sediments. Additionally, these sedimentary archives can potentially provide another record of globally reducing conditions for intervals of expansive global anoxia (i.e., −2.0 value is recorded), as found in various ancient studies using Tl isotopes (Ostrander et al., 2017, 2019, 2023; Them et al., 2018; Bowman et al., 2019; Newby et al., 2021; Li et al., 2021; Kozik et al., 2022, 2023; Heard et al., 2023). However, when the oceans have a similar extent of oxic bottom waters as found today, the most extreme value for any suboxic sedimentary record would not be able to properly represent an oxic signal of −6, having only an isotopic value of −4.0. With such considerations, all low-oxygen settings may be a record for ancient seawater Tl isotopic composition, but with caution in local redox interpretation. Additionally, ancient sediments that do not have the full isotopic range found in modern sediments and have uncertain local redox signatures may be indicative of these suboxic sediments that only record a muted isotopic signal.

4.3. Updating the thallium mass balance

The data presented here as well as other recent work (Wang et al., 2022) indicate that some modifications may need to occur to the thallium mass balance compared to older reviews on this system (Nielsen et al., 2017; Owens, 2019); however, the modification we offer is minor. A new compilation of previously measured Tl isotopes pertinent to the seawater isotopic mass balance has also been done to better constrain this isotopic system and understand the placement of this new data from the California, Mexico, and Peru Margins (Fig. 7). Taking into account the refinement of the suboxic and anoxic settings in which Tl can be recorded (Fig. 7b) and recent work better constraining the fluxes of reducing sinks (Wang et al., 2022), several changes can be made that more accurately represent the mass balance (Fig. 8).
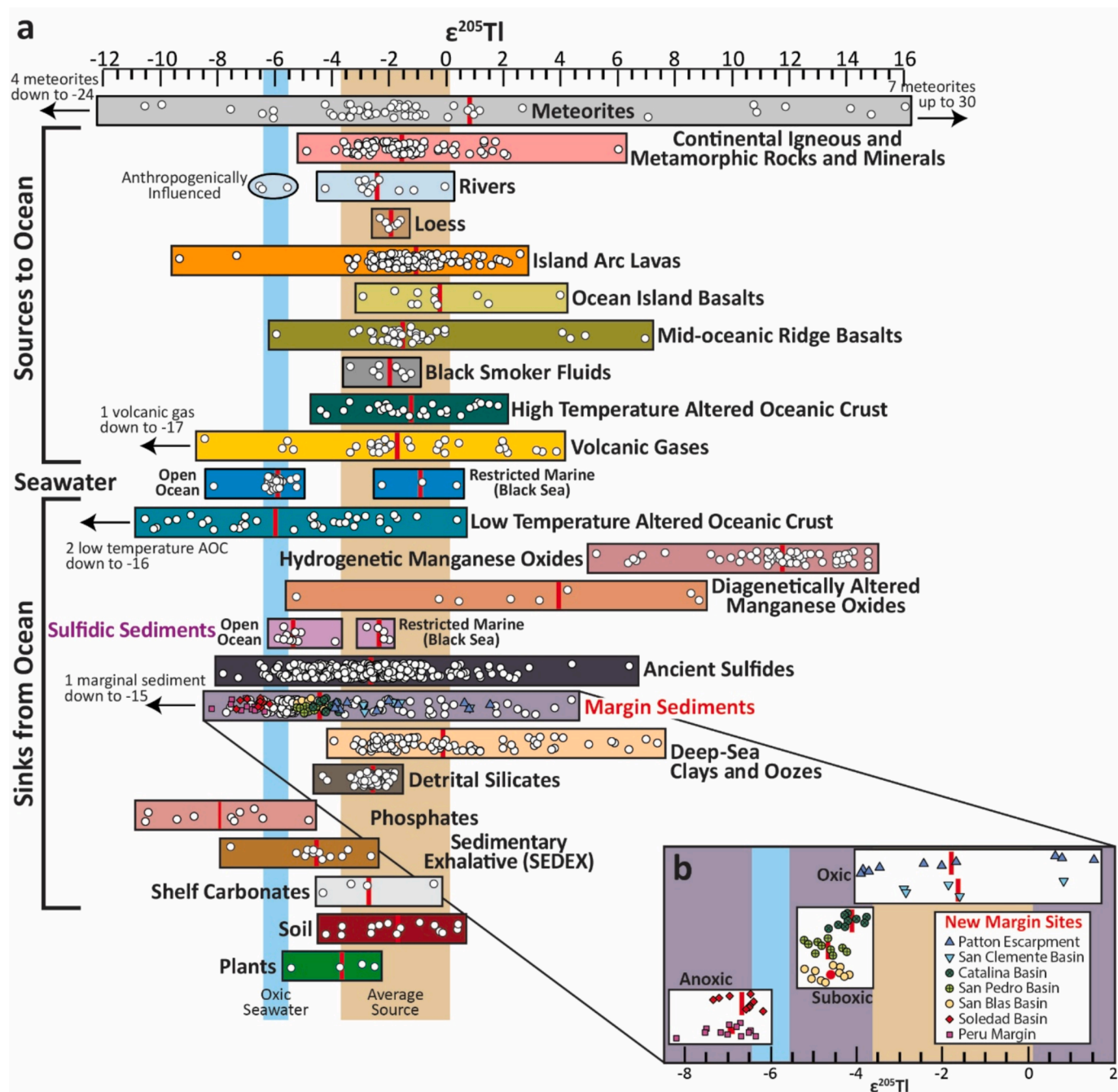
Fig. 7. (a) Complete flux and reservoir data for Tl isotopes, divided up by major fluxes and seawater reservoir (Rehkämper et al., 2002; Rehkämper and Nielsen, 2004; Nielsen et al., 2005, 2006a, c, b, 2007, 2011, 2015, 2016; Baker et al., 2009, 2010b, a; Prytulak et al., 2013; Wickham, 2014; Coggon et al., 2014; Hettmann et al., 2014b, a; Kersten et al., 2014; Ostrander et al., 2017, 2019; Owens et al., 2017; Shu et al., 2017; Palk et al., 2018; Peter et al., 2018; Them et al., 2018; Turner, 2018; Bowman et al., 2019; Fan et al., 2020; Newby et al., 2021; Rader et al., 2021; Li et al., 2021; Kozik et al., 2023; Wang et al., 2022; Kozik et al., 2022). Large colored boxes represent the full range of isotopic compositions measured for the particular flux or reservoir, with black label of the flux/reservoir to the side. Small white circles represent isotopic composition of each individual data point within that flux. Average isotopic composition of each flux or reservoir is highlighted as a red bar within the larger box. It should be noted that these are mean averages of all available data and are not weighted in favor of samples that may be more representative of typical conditions for the flux or reservoir; thus, averages presented here are not necessarily equivalent to average fluxes' isotopic values for the mass balance (Fig. 8). Fluxes are divided primarily into sources to the ocean (top) and sinks from the ocean (bottom), as well as some other studied fluxes and reservoirs (i.e., meteorites, seawater, soil, plants). Several fluxes may be combined together or ignored due to being too trace to affect final mass balance (Fig. 8). Some ranges have extreme outliers that are labeled along the edges to the figure. Certain boxes are subdivided, such as the differences in open versus restricted marine settings, or in the case for riverine, separating out the highly anthropogenically affected isotopic values due to their inaccessibility for paleoredox mass balance calculations. Previous work shows that sediments deposited under euxinic settings (purple label) maintain seawater values (Owens et al., 2017), hence the similarities in values with the seawater boxes. The margin sediments (red label) for this study along with other recently studied marginal sediment core tops (Wang et al., 2022) have an inset (b) that shows the range of values for this study. This flux covers various bottom water redox states. Additionally, the data points for this study are colored and shaped to match Fig. 1. The inset also shows the range and average composition at each site, grouping together oxic (Patton Escarpment and San Clemente Basin), 'suboxic' (Catalina Basin, San Pedro Basin, and San Blas Basin), and anoxic basins (Soledad Basin and all Peru Margin samples). AOC = altered oceanic crust.
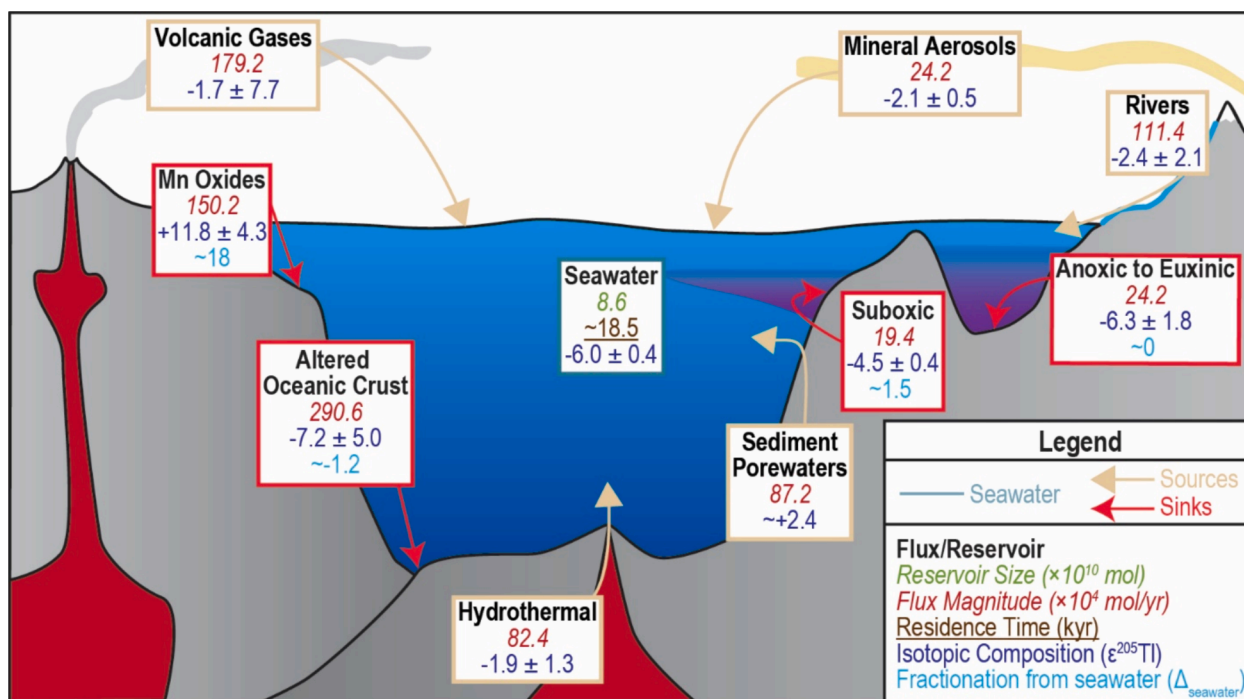
Fig. 8. A revised mass balance of Tl isotopes (Nielsen et al., 2017; Owens, 2019; Li et al., 2021). This mass balance uses better constraints on the isotopic composition of suboxic settings as defined by this study, improved flux estimates on the suboxic and anoxic to euxinic sediment fluxes (Wang et al., 2022), and generally more precise isotopic compositions for all fluxes based on new averages (Fig. 7). Legend in bottom right corner with font and color used to differentiate various flux sizes and isotopic values of the reservoir and fluxes. Errors are 2σ of the compiled isotopic values.

New averages for isotope composition and errors were determined by the compilation (Fig. 7), but these are not significantly different from previous calculations (Nielsen et al., 2017; Owens, 2019) outside the two minor sinks that were the focus of this study. The euxinic sink remains the same with the addition of anoxia assuming raised sulfide content (Fan et al., 2020). This study and Wang et al. (2022) show that some extra caution should be made in this decision depending on other indicators for local redox. This study prescribes an isotopic value of ~ -4.5 to the suboxic sink, greatly refining the large range previously utilized of -6.0 to 0.0. This indicates a slight positive fractionation from seawater. This offset means suboxic sediments could be used in deep time to note fluctuations in Tl isotopes but not original seawater isotopic composition. As differentiating between suboxic and anoxic sediments is difficult in the geologic past, it is reasonable to be cautious about interpretations of anoxic sedimentary records since these may be suboxic and not recording a full range of Tl isotopic variation. Thus, if local redox proxies are ambiguous, it becomes imperative to analyze more than one section if possible.

Wang et al. (2022) has shown that the fluxes of reducing conditions may be a higher proportion of the total output flux of the ocean than previously estimated, indicating doubling of the anoxic-euxinic sink. However, that study shows most of the flux increase is from the California Margin sediments, which this study indicates are mostly suboxic, supported by Wang et al. (2022)'s values for the majority of California Margin core tops matching our manganous-ferruginous sediments. Hence, the suboxic flux has been increased from <1 % to 4 % and the anoxic-euxinic flux has been increased from 4 % to 5 % of the total output flux (Fig. 8). To account for these changes, the Mn oxide burial sink and low temperature alteration of oceanic crust sink have both been decreased in equal proportions, though both remain the greater output fluxes.

One last area of note for this updated mass balance is a more positive isotopic value for the porewater flux, which supplies Tl to seawater. This unconstrained flux is assumed to be related to the dissolution of Mn oxides, however, data remains limited on the size of that remobilization

flux (Owens, 2019). To maintain a steady state with this new mass balance, the isotopic composition of this flux was made more positive, from 0.0 to $+2.4$, now being the most isotopically distinct source flux (Figs. 7 and 8). There is a slight change to average source isotopic compositions due to this from ~ 2.0 to -1.8 ± 1.9. This change matches the previous assumption of its relation to Mn oxide dissolution. However, more work is needed to continue to improve this flux and the overall Tl isotope paleoproxy and the factors that could control it over time.

5. Conclusions

Thallium isotopes under reducing conditions are becoming a useful means of constraining global paleoredox conditions, though better understanding is required to determine the local reducing conditions in which Tl isotopes are recorded. Improving this marine isotope system is most important when utilizing suboxic sediments, which, until this study, consisted of few available data points (Rehkämper et al., 2004; Nielsen et al., 2011) compared to many of the other known fluxes and reservoirs of Tl (Fig. 7). However, recent studies may have additional samples under 'suboxic' conditions that were not described as such (Wang et al., 2022). After studying open ocean sites in the California, Mexico, and Peru Margins for local redox conditions, additional information can be applied to how Tl isotopes are recorded in the authigenic component, especially under more 'suboxic' environments, defined as manganous-ferruginous based on porewater enrichments.

The most oxic settings tend to record the most positive Tl isotopic compositions, trending with changes in sedimentary Mn content. Meanwhile, suboxic manganous-ferruginous sections record a mixed signature that is slightly more positive than seawater isotopic values while still more negative than marine input values. Lastly are the anoxic sections, which accurately record seawater composition, confirming previous research into anoxic and euxinic environments (Owens et al., 2017; Fan et al., 2020). This data also shows that under reducing conditions, diagenetic changes to the signal are minimal. Hence, euxinic

sediments are the best archive for ancient seawater reconstruction (Nielsen et al., 2011; Owens et al., 2017), but anoxic sediments with little sedimentary Mn (<1000 ppm) and elevated pyrite ($Fe_{py}/Fe_{HR} > 0.35$) can also be used as suspected by previous research (Fan et al., 2020; Wang et al., 2022). Meanwhile, suboxic sediments record an offset seawater isotopic signature, indicating they can be used to determine first order changes in deep-time paleoredox interpretations but do not represent original seawater compositions.

Data availability

Data are available through Mendeley Data Repository at https://doi.org/10.17632/4nsszmjjss.2.

CRediT authorship contribution statement

Sean M. Newby: Writing – review & editing, Writing – original draft, Visualization, Validation, Resources, Investigation, Formal analysis, Data curation, Conceptualization. **Siqi Li:** Writing – review & editing, Validation, Investigation, Data curation. **Silke Severmann:** Supervision, Resources, Project administration, Funding acquisition. **James McManus:** Writing – review & editing, Supervision, Project administration, Funding acquisition. **Florian Scholz:** Writing – review & editing, Resources. **Jeremy D. Owens:** Writing – review & editing, Supervision, Resources, Project administration, Funding acquisition, Conceptualization.

Declaration of competing interest

The authors declare that they have no known competing financial interests or personal relationships that could have appeared to influence the work reported in this paper.

Acknowledgements

Appendix A. Supplementary material

Additional supplementary material is included with this manuscript. This includes supplemental methods to discuss additional procedures utilized for additional clarification of material as well as a supplemental results and discussion section, which describes the results of the additional methods and interprets them as well as additional points that may be considered for the data set as a whole. In addition, there are two tables for the additional results and six figures to display additional data and comparisons of data sets. Lastly, an additional list of references is included with this supplementary material.

Supplementary material to this article can be found online at https://doi.org/10.1016/j.gca.2025.08.020.

References

Algeo, T.J., Maynard, J.B., 2004. Trace-element behavior and redox facies in core shales of Upper Pennsylvanian Kansas-type cyclothems. Chem. Geol. 206, 289–318.

Baker, R.G.A., Rehkämper, M., Hinkley, T.K., Nielsen, S.G., Toutain, J.P., 2009. Investigation of thallium fluxes from subaerial volcanism-Implications for the present and past mass balance of thallium in the oceans. Geochim. Cosmochim. Acta 73, 6340–6359.

Baker, R.G.A., Rehkämper, M., Ihlenfeld, C., Oates, C.J., Coggon, R., 2010a. Thallium isotope variations in an ore-bearing continental igneous setting: Collahuasi Formation, northern Chile. Geochim. Cosmochim. Acta 74, 4405–4416.

Baker, R.G.A., Schönbächler, M., Rehkämper, M., Williams, H.M., Halliday, A.N., 2010b. The thallium isotope composition of carbonaceous chondrites - new evidence for live 205Pb in the early solar system. Earth Planet. Sci. Lett. 291, 39–47.

Barnett, P.R.O., Watson, J., Connelly, D., 1984. A multiple corer for taking virtually undisturbed samples from shelf, bathyal and abyssal sediments. Oceanol. Acta 7, 399–404.

Berelson, W.M., Hammond, D.E., Johnson, K.S., 1987. Benthic fluxes and the cycling of biogenic silica and carbon in two southern California borderland basins. Geochim. Cosmochim. Acta 51, 1345–1363.

Berelson, W.M., Prokopenko, M., Sansone, F.J., Graham, A.W., McManus, J., Bernhard, J. M., 2005. Anaerobic diagenesis of silica and carbon in continental margin sediments: discrete zones of TCO2 production. Geochim. Cosmochim. Acta 69, 4611–4629.

Berner, R.A., 2001. Modeling atmospheric O2 over Phanerozoic time. Geochim. Cosmochim. Acta 65, 685–694.

Bond, D.P.G., Grasby, S.E., 2017. On the causes of mass extinctions. Palaeogeogr. Palaeoclimatol. Palaeoecol. 478, 3–29.

Böning, P., Brumsack, H.J., Böttcher, M.E., Schnetger, B., Kriete, C., Kallmeyer, J., Borchers, S.L., 2004. Geochemistry of Peruvian near-surface sediments. Geochim. Cosmochim. Acta 68, 4429–4451.

Bowman, C.N., Young, S.A., Kaljo, D., Eriksson, M.E., Them, T.R., Hints, O., Martma, T., Owens, J.D., 2019. Linking the progressive expansion of reducing conditions to a stepwise mass extinction event in the late Silurian oceans. Geology 47, 968–972.

Bruggmann, S., Severmann, S., McManus, J., 2023. Geochemical conditions regulating chromium preservation in marine sediments. Geochim. Cosmochim. Acta 348, 239–257.

Canfield, D.E., Poulton, S.W., Narbonne, G.M., 2007. Late-Neoproterozoic deep-ocean oxygenation and the rise of animal life. Sci. (80-.) 315, 92–95.

Chen, X., Li, S., Newby, S.M., Lyons, T.W., Wu, F., Owens, J.D., 2021. Iron and manganese shuttle has no effect on sedimentary thallium and vanadium isotope signatures in Black Sea sediments. Geochim. Cosmochim. Acta 317, 218–233.

Chong, L.S., Prokopenko, M.G., Berelson, W.M., Townsend-Small, A., McManus, J., 2012. Nitrogen cycling within suboxic and anoxic sediments from the continental margin of Western North America. Mar. Chem. 128–129, 13–25.

Coggon, R.M., Rehkämper, M., Atteck, C., Teagle, D.A.H., Alt, J.C., Cooper, M.J., 2014. Controls on thallium uptake during hydrothermal alteration of the upper ocean crust. Geochim. Cosmochim. Acta 144, 25–42.

Fan, H., Nielsen, S.G., Owens, J.D., Auro, M., Shu, Y., Hardisty, D.S., Horner, T.J., Bowman, C.N., Young, S.A., Wen, H., 2020. Constraining oceanic oxygenation during the Shuram excursion in South China using thallium isotopes. Geobiology 18, 348–365.

Froelich, P.N., Klinkhammer, G.P., Bender, M.L., Luedtke, N.A., Heath, G.R., Cullen, D., Dauphin, P., Hammond, D., Hartman, B., Maynard, V., 1979. Early oxidation of organic matter in pelagic sediments of the eastern equatorial Atlantic: suboxic diagenesis. Geochim. Cosmochim. Acta 43, 1075–1090.

Hansel, C.M., 2017. Manganese in Marine Microbiology. In: Advances in Microbial Physiology, pp. 37–83.

Hardisty, D.S., Lu, Z., Planavsky, N.J., Bekker, A., Philippot, P., Zhou, X., Lyons, T.W., 2014. An iodine record of Paleoproterozoic surface ocean oxygenation. Geology 42, 619–622.

Hardisty, D.S., Lyons, T.W., Riedinger, N., Isson, T.T., Owens, J.D., Aller, R.C., Rye, D.M., Planavsky, N.J., Reinhard, C.T., Gill, B.C., Masterson, A.L., Asael, D., Johnston, D.T., 2018. An evaluation of sedimentary molybdenum and iron as proxies for pore fluid paleoredox conditions. Am. J. Sci. 318, 527–556.

Heard, A.W., Wang, Y., Ostrander, C.M., Auro, M., Canfield, D.E., Zhang, S., Wang, H., Wang, X., Nielsen, S., 2023. Coupled vanadium and thallium isotope constraints on Mesoproterozoic ocean oxygenation around 1.38-1.39 Ga. Earth Planet. Sci. Lett. 610, 118127.

Hettmann, K., Kreissig, K., Rehkämper, M., Wenzel, T., Mertz-Kraus, R., Markl, G., 2014a. Thallium geochemistry in the metamorphic Lengenbach sulfide deposit, switzerland: Thallium-isotope fractionation in a sulfide melt. Am. Mineral. 99, 793–803.

Hettmann, K., Marks, M.A.W., Kreissig, K., Zack, T., Wenzel, T., Rehkämper, M., Jacob, D.E., Markl, G., 2014b. The geochemistry of Tl and its isotopes during magmatic and hydrothermal processes: the peralkaline Ilimaussaq complex, southwest Greenland. Chem. Geol. 366, 1–13.

Kendall, B., Dahl, T.W., Anbar, A.D., 2017. The stable isotope geochemistry of molybdenum. Rev. Mineral. Geochem. 82, 683–732.

Kersten, M., Xiao, T., Kreissig, K., Brett, A., Coles, B.J., Rehkämper, M., 2014. Tracing anthropogenic thallium in soil using stable isotope compositions. Environ. Sci. Technol. 48, 9030–9036.

Kozik, N.P., Young, S.A., Lindskog, A., Ahlberg, P., Owens, J.D., 2023. Protracted oxygenation across the Cambrian–Ordovician transition: a key initiator of the Great Ordovician Biodiversification event? Geobiology 1–18.

Kozik, N.P., Young, S.A., Newby, S.M., Liu, M., Chen, D., Hammarlund, E.U., Bond, D.P. G., Them, T.R., Owens, J.D., 2022. Rapid marine oxygen variability: driver of the late Ordovician mass extinction. Sci. Adv. 8, 1–9.

Lau, K.V., Romaniello, S.J., Zhang, F., 2019. *The Uranium Isotope Paleoredox Proxy*. Cambridge University Press.

Leslie, B.W., Hammond, D.E., Berelson, W.M., Lund, S.P., 1990. Diagenesis in anoxic sediments from the California continental borderland and its influence on iron, sulfur, and magnetite behavior. J. Geophys. Res. 95, 4453–4470.

Li, Z., Cole, D.B., Newby, S.M., Owens, J.D., Kendall, B., Reinhard, C.T., 2021. New constraints on mid-Proterozoic ocean redox from stable thallium isotope systematics of black shales. Geochim. Cosmochim. Acta 315, 185–206.

Liu, W., Hao, J., Elzinga, E.J., Piotrowiak, P., Nanda, V., Yee, N., Falkowski, P.G., 2020. Anoxic photogeochemical oxidation of manganese carbonate yields manganese oxide. Proc. Natl. Acad. Sci. USA 117, 22698–22704.

Lu, Z., Jenkyns, H.C., Rickaby, R.E.M., 2010. Iodine to calcium ratios in marine carbonate as a paleo-redox proxy during oceanic anoxic events. Geology 38, 1107–1110.

Lyons, T.W., Reinhard, C.T., Planavsky, N.J., 2014. The rise of oxygen in Earth's early ocean and atmosphere. Nature 506, 307–315.

Mclennan, S.M., 2001. Relationships between the trace element composition of sedimentary rocks and upper continental crust. Geochem. Geophys. Geosyst. 2.

McManus, J., Berelson, W.M., Coale, K.H., Johnson, K.S., Kilgore, T.E., 1997. Phosphorus regeneration in continental margin sediments. Geochim. Cosmochim. Acta 61, 2891–2907.

McManus, J., Berelson, W.M., Klinkhammer, G.P., Johnson, K.S., Coale, K.H., Anderson, R.F., Kumar, N., Burdige, D.J., Hammond, D.E., Brumsack, H.J., McCorkle, D.C., Rushdi, A., 1998. Geochemistry of barium in marine sediments: implications for its use as a paleoproxy. Geochim. Cosmochim. Acta 62, 3453–3473.

McManus, J., Berelson, W.M., Severmann, S., Johnson, K.S., Hammond, D.E., Roy, M., Coale, K.H., 2012. Benthic manganese fluxes along the Oregon–California continental shelf and slope. Cont. Shelf Res. 43, 71–85.

Newby, S.M., Owens, J.D., Schoepfer, S.D., Algeo, T.J., 2021. Transient ocean oxygenation at end-Permian mass extinction onset shown by thallium isotopes. Nat. Geosci. 14, 678–683.

Nielsen, S.G., 2021. Vanadium Isotopes. In: Geochemical Tracers in Earth System Science. Cambridge University Press, Cambridge, pp. 1–24.

Nielsen, S.G., Goff, M., Hesselbo, S.P., Jenkyns, H.C., LaRowe, D.E., Lee, C.T.A., 2011. Thallium isotopes in early diagenetic pyrite - a paleoredox proxy? Geochim. Cosmochim. Acta 75, 6690–6704.

Nielsen, S.G., Klein, F., Kading, T., Blusztajn, J., Wickham, K., 2015. Thallium as a tracer of fluid-rock interaction in the shallow Mariana forearc. Earth Planet. Sci. Lett. 430, 416–426.

Nielsen, S.G., Mar-Gerrison, S., Gannoun, A., LaRowe, D., Klemm, V., Halliday, A.N., Burton, K.W., Hein, J.R., 2009. Thallium isotope evidence for a permanent increase in marine organic carbon export in the early Eocene. Earth Planet. Sci. Lett. 278, 297–307.

Nielsen, S.G., Rehkämper, M., Baker, J., Halliday, A.N., 2004. The precise and accurate determination of thallium isotope compositions and concentrations for water samples by MC-ICPMS. Chem. Geol. 204, 109–124.

Nielsen, S.G., Rehkämper, M., Brandon, A.D., Norman, M.D., Turner, S., O'Reilly, S.Y., 2007. Thallium isotopes in Iceland and Azores lavas - implications for the role of altered crust and mantle geochemistry. Earth Planet. Sci. Lett. 264, 332–345.

Nielsen, S.G., Rehkämper, M., Halliday, A.N., 2006a. Large thallium isotopic variations in iron meteorites and evidence for lead-205 in the early solar system. Geochim. Cosmochim. Acta 70, 2643–2657.

Nielsen, S.G., Rehkämper, M., Norman, M.D., Halliday, A.N., Harrison, D., 2006b. Thallium isotopic evidence for ferromanganese sediments in the mantle source of Hawaiian basalts. Nature 439, 314–317.

Nielsen, S.G., Rehkämper, M., Porcelli, D., Andersson, P., Halliday, A.N., Swarzenski, P. W., Latkoczy, C., Günther, D., 2005. Thallium isotope composition of the upper continental crust and rivers - an investigation of the continental sources of dissolved marine thallium. Geochim. Cosmochim. Acta 69, 2007–2019.

Nielsen, S.G., Rehkämper, M., Prytulak, J., 2017. Investigation and application of thallium isotope fractionation. Rev. Mineral. Geochem. 82, 759–798.

Nielsen, S.G., Rehkämper, M., Teagle, D.A.H., Butterfield, D.A., Alt, J.C., Halliday, A.N., 2006c. Hydrothermal fluid fluxes calculated from the isotopic mass balance of thallium in the ocean crust. Earth Planet. Sci. Lett. 251, 120–133.

Nielsen, S.G., Wasylenki, L.E., Rehkämper, M., Peacock, C.L., Xue, Z., Moon, E.M., 2013. Towards an understanding of thallium isotope fractionation during adsorption to manganese oxides. Geochim. Cosmochim. Acta 117, 252–265.

Nielsen, S.G., Yogodzinski, G., Prytulak, J., Plank, T., Kay, S.M., Kay, R.W., Blusztajn, J., Owens, J.D., Auro, M., Kading, T., 2016. Tracking along-arc sediment inputs to the Aleutian arc using thallium isotopes. Geochim. Cosmochim. Acta 181, 217–237.

Noffke, A., Hensen, C., Sommer, S., Scholz, F., Bohlen, L., Mosch, T., Graco, M., Wallmann, K., 2012. Benthic iron and phosphorus fluxes across the Peruvian oxygen minimum zone. Limnol. Oceanogr. 57, 851–867.

Olesen, K.P., Nielsen, S.G., Ostrander, C.M., Udy, N., Canfield, D.E., 2025. Thallium cycling and boundary exchange in a continental margin basin. Geochim. Cosmochim. Acta.

Ostrander, C.M., Heard, A.W., Swanner, E.D., Shu, Y., Zheng, W., Zhao, Y., Nielsen, S.G., 2025. Thallium isotope cycling in a ferruginous Precambrian ocean analogue. Geochim. Cosmochim. Acta 390, 264–275.

Ostrander, C.M., Nielsen, S.G., Gadol, H.J., Villarroel, L., Wankel, S.D., Horner, T.J., Blusztajn, J., Hansel, C.M., 2023. Thallium isotope cycling between waters, particles, and sediments across a redox gradient. Geochim. Cosmochim. Acta 348, 397–409.

Ostrander, C.M., Nielsen, S.G., Owens, J.D., Kendall, B., Gordon, G.W., Romaniello, S.J., Anbar, A.D., 2019. Fully oxygenated water columns over continental shelves before the Great Oxidation event. Nat. Geosci. 12, 186–192.

Ostrander, C.M., Owens, J.D., Nielsen, S.G., 2017. Constraining the rate of oceanic deoxygenation leading up to a cretaceous Oceanic Anoxic event (OAE-2: ~94 Ma). Sci. Adv. 3, e1701020.

Ostrander, C.M., Shu, Y., Nielsen, S.G., Dellwig, O., Blusztajn, J., Schulz-Vogt, H.N., Hübner, V., Hansel, C.M., 2024. Anthropogenic forcing of the Baltic Sea thallium cycle. Environ. Sci. Technol. 58, 8510–8517.

Owens, J.D., 2019. Application of Thallium Isotopes: Tracking Marine Oxygenation through Manganese Oxide Burial. In: Elements in Geochemical Tracers in Earth System Science. Science Cambridge University Press, Cambridge, pp. 1–12.

Owens, J.D., Nielsen, S.G., Horner, T.J., Ostrander, C.M., Peterson, L.C., 2017. Thallium-isotopic compositions of euxinic sediments as a proxy for global manganese-oxide burial. Geochim. Cosmochim. Acta 213, 291–307.

Palk, C., Andreasen, R., Rehkämper, M., Stunt, A., Kreissig, K., Coles, B., Schönbächler, M., Smith, C., 2018. Variable Tl, Pb, and Cd concentrations and isotope compositions of enstatite and ordinary chondrites—evidence for volatile element mobilization and decay of extinct205Pb. Meteorit. Planet. Sci. 53, 167–186.

Peter, J.M., Gadd, M.G., Layton-Matthews, D., Voinot, A., 2018. Reconnaissance thallium isotope study of zinc-lead SEDEX mineralization and host rocks in the Howard's Pass district, Selwyn Basin, Yukon: potential application to paleoredox determinations and fingerprinting of mineralization. Geol. Surv. Canada, Open File 8358, 173–191.

Phillips, R.F., Wang, Y., Klein, F., Farfan, G., Ostrander, C.M., Gadol, H., Hansel, C.M., Nielsen, S.G., 2023. The role of manganese oxide mineralogy in thallium isotopic fractionation upon sorption. Geochim. Cosmochim. Acta 356, 83–92.

Poulson, R.L., Siebert, C., McManus, J., Berelson, W.M., 2006. Authigenic molybdenum isotope signatures in marine sediments. Geology 34, 617–620.

Poulton, S.W., Canfield, D.E., 2011. Ferruginous conditions: a dominant feature of the ocean through Earth's history. Elements 7, 107–112.

Poulton, S.W., Canfield, D.E., 2005. Development of a sequential extraction procedure for iron: implications for iron partitioning in continentally derived particulates. Chem. Geol. 214, 209–221.

Prytulak, J., Nielsen, S.G., Plank, T., Barker, M., Elliott, T., 2013. Assessing the utility of thallium and thallium isotopes for tracing subduction zone inputs to the Mariana arc. Chem. Geol. 345, 139–149.

Rader, S.T., Gaschnig, R.M., Newby, S.M., Bebout, G.E., Mirakian, M.J., Owens, J.D., 2021. Thallium behavior during high-pressure metamorphism in the Western Alps, Europe. Chem. Geol. 579, 120349.

Rader, S.T., Maier, R.M., Barton, M.D., Mazdab, F.K., 2019. Uptake and Fractionation of Thallium by Brassica juncea in a Geogenic Thallium-Amended Substrate. Environ. Sci. Technol. 53, 2441–2449.

Raiswell, R., Hardisty, D.S., Lyons, T.W., Canfield, D.E., Owens, J.D., Planavsky, N.J., Poulton, S.W., Reinhard, C.T., 2018. The iron paleoredox proxies: a guide to the pitfalls, problems and proper practice. Am. J. Sci. 318, 491–526.

Rehkämper, M., Frank, M., Hein, J.R., Halliday, A., 2004. Cenozoic marine geochemistry of thallium deduced from isotope studies of ferromanganese crusts and pelagic sediments. Earth Planet. Sci. Lett. 219, 77–91.

Rehkämper, M., Frank, M., Hein, J.R., Porcelli, D., Halliday, A., Ingri, J., Liebetrau, V., 2002. Thallium isotope variations in seawater and hydrogenetic, diagenetic, and hydrothermal ferromanganese deposits. Earth Planet. Sci. Lett. 197, 65–81.

Rehkämper, M., Nielsen, S.G., 2004. The mass balance of dissolved thallium in the oceans. Mar. Chem. 85, 125–139.

Reimers, C.E., Fischer, K.M., Merewether, R., Smith, K.L., Jahnke, R.A., 1986. Oxygen microprofiles measured in situ in deep ocean sediments. Nature 320, 741–744.

Rue, E.L., Smith, G.J., Cutter, G.A., Bruland, K.W., 1994. The response of trace-element redox couples to suboxic conditions in the water column. Deep Res. Part I Oceanogr. Res. Pap. 44, 113–134.

Scholz, F., Hardisty, D.S., Dale, A.W., 2024. Early diagenetic controls on sedimentary iodine release and iodine-to-organic carbon ratios in the paleo-record. Global Biogeochem. Cycles 38.

Scholz, F., Hensen, C., Noffke, A., Rohde, A., Liebetrau, V., Wallmann, K., 2011. Early diagenesis of redox-sensitive trace metals in the Peru upwelling area - response to ENSO-related oxygen fluctuations in the water column. Geochim. Cosmochim. Acta 75, 7257–7276.

Scholz, F., Severmann, S., McManus, J., Hensen, C., 2014a. Beyond the Black Sea paradigm: the sedimentary fingerprint of an open-marine iron shuttle. Geochim. Cosmochim. Acta 127, 368–380.

Scholz, F., Severmann, S., McManus, J., Noffke, A., Lomnitz, U., Hensen, C., 2014b. On the isotope composition of reactive iron in marine sediments: Redox shuttle versus early diagenesis. Chem. Geol. 389, 48–59.

Seeberg-Elverfeldt, J., Schluter, M., Feseker, T., Kolling, M., 2005. Rhizon sampling of porewaters near the sediment-water interface of aquatic systems. Limnol. Oceanogr. Methods 3, 361–371.

Shu, Y., Nielsen, S.G., Zeng, Z., Shinjo, R., 2017. Tracing subducted sediment inputs to the Ryukyu arc-Okinawa Trough system: evidence from thallium isotopes. Geochim. Cosmochim. Acta 217, 462–491.

Them, T.R., Gill, B.C., Caruthers, A.H., Gerhardt, A.M., Gröcke, D.R., Lyons, T.W., Marroquín, S.M., Nielsen, S.G., João, P.T.A., Owens, J.D., 2018. Thallium isotopes reveal protracted anoxia during the Toarcian (Early Jurassic) associated with volcanism, carbon burial, and mass extinction. PNAS 115, 6596–6601.

Tribovillard, N., Algeo, T.J., Lyons, T., Riboulleau, A., 2006. Trace metals as paleoredox and paleoproductivity proxies: an update. Chem. Geol. 232, 12–32.

Turner, K.M., 2018. Florida State University Libraries A Geochemical Analysis of Rare Earth Elements Associated with Significant Sedimentary Phosphate Deposits of West- . Florida State University.

Tyson, R.V., Pearson, T.H., 1991. Modern and ancient continental shelf anoxia. Geol. Soc. Spec. Publ. 1–24.

Wang, Y., Lu, W., Costa, K.M., Nielsen, S.G., 2022. Beyond anoxia: exploring sedimentary thallium isotopes in paleo-redox reconstructions from a new core top collection. Geochim. Cosmochim. Acta in Revisio 347–361.

Wickham, K., 2014. Thallium Isotope Implications for the Metalliferous Source of Carlin-type Deposits in northern Nevada by. University of Nevada.

Wu, F., Owens, J.D., Huang, T., Sarafian, A., Huang, K.F., Sen, I.S., Horner, T.J., Blusztajn, J., Morton, P., Nielsen, S.G., 2019. Vanadium isotope composition of seawater. Geochim. Cosmochim. Acta 244, 403–415.